

Kinetic principles underlying pioneer function of GAGA transcription factor in live cells

Xiaona Tang¹, Taibo Li^{1,2}, Sheng Liu¹, Jan Wisniewski³, Qinsi Zheng⁴, Yikang Rong⁵,
Luke D. Lavis⁴, Carl Wu^{1,6,*}

1. Department of Biology, Johns Hopkins University, Baltimore, USA
2. Department of Biomedical Engineering, Johns Hopkins University, Baltimore, USA
3. Experimental Immunology Branch, National Cancer Institute, Bethesda, USA
4. Janelia Research Campus, Howard Hughes Medical Institute, Ashburn, United States
5. State Key Laboratory of Bio-control, Institute of Entomology, School of Life Sciences, Sun Yat-sen University, Guangzhou, China
6. Department of Molecular Biology and Genetics, Johns Hopkins School of Medicine, Baltimore, United States

*Correspondence: wuc@jhu.edu

Keywords: transcription/chromatin accessibility/pioneer factor/single-particle tracking/heat shock

Abstract

How pioneer factors interface with chromatin to promote accessibility for transcription control is poorly understood *in vivo*. Here, we directly visualize chromatin association by the prototypical GAGA pioneer factor (GAF) in live *Drosophila* hemocytes. Single-particle tracking reveals that the majority of GAF is chromatin-bound, with a stable-binding fraction showing nucleosome-like confinement residing on chromatin for over 2 minutes, far longer than the dynamic range of most transcription factors. These kinetic properties require the full complement of GAF's DNA-binding, multimerization and intrinsically disordered domains, and are autonomous from recruited chromatin remodelers NURF and PBAP, whose activities primarily benefit GAF's neighbors such as HSF. Evaluation of GAF kinetics together with its endogenous abundance indicates that despite on-off dynamics, GAF constitutively and fully occupies chromatin targets, thereby providing a temporal mechanism that sustains open chromatin for transcriptional responses to homeostatic, environmental, and developmental signals.

Introduction

Drosophila GAGA factor (GAF), a ubiquitous and essential Zn finger transcription factor (TF) encoded by the *Trithorax-like (Trl)* gene, is a multimeric protein complex that binds specifically to clusters of adjacent GAGAG sequences on numerous genes, including homeotic, steroid- and heat shock-response genes¹⁻⁴. GAF regulates transcription by interactions with the TAF3 and TAF4 components of the TFIID general transcription factor⁵⁻⁷, the NELF elongation factor⁸, and antagonism to histone H1-mediated transcriptional repression⁹. In addition, as a pioneer transcription factor^{10,11}, GAF is capable of binding to reconstituted nucleosomes¹², directly recruiting chromatin remodelers NURF, PBAP and other factors^{6,13-15} to create accessible chromatin for neighboring non-pioneer factors¹⁶ and assembly of the paused RNA Polymerase II (Pol II)^{17,18}. Beneficiaries of GAF pioneering activity in *Drosophila* include - heat shock factor HSF¹⁹, coactivator CBP^{19,20}, Polycomb repressor PHO (Pleiohomeotic)²¹, and the insulator binding complex LBC (Large Boundary Complex)²².

Genome-wide analysis reveals that GAF is enriched *in vivo* at promoters as well as distal *cis*-regulatory regions comprising several thousand targets which often include clusters of tandem GA repeats^{17,23,24}. GAF-specific RNA or protein depletion experiments have importantly demonstrated the *in vivo* function of GAF in generating chromatin accessibility in the *Drosophila* embryo and in cultured cells^{17,18,24,25}. Despite these advances over decades of research, unifying principles for pioneering activity of TFs such as GAF have remained elusive. How pioneer factors differ from other sequence-specific transcription factors and the kinetic mechanisms by which pioneers perform their key genomic functions are subjects of continuing debate.

To elucidate the underlying mechanisms of this pleiotropic transcription factor, we have studied the kinetics of GAF diffusion in the nucleoplasm and on genomic chromatin by single-particle

tracking (SPT) in live *Drosophila* hemocytes under different genetic contexts. In comparison, we also measured the kinetic parameters for HSF at normal and heat-stressed conditions. We then determined GAF and HSF protein levels in hemocytes, curated existing databases for numbers of genomic targets and integrated these parameters with the measured kinetics to obtain the target occupancy of each factor in vivo. Our findings uncover crucial quantitative principles for pioneering and maintaining chromatin accessibility over extended time periods even when the responsible factors continuously bind to and dissociate from their chromatin targets in a dynamic manner.

Results

GAF imaging quantifies major chromatin binding fractions and prolonged residence times

Drosophila Trl encodes two isoforms of GAF that harbor the N-terminal POZ/BTB domain (hereafter called POZ), the central zinc-finger (ZF)-containing DNA binding domain (DBD), and long and short C-terminal Q-rich domains (**Fig. 1A**)^{4,26}. We used CRISPR-Cas9-based gene editing to insert a HaloTag at the N-terminus of endogenous *Trl* (**Fig. 1A** and **Fig. S1A-D**). The Halo knock-in strain is homozygous-viable, expressing long and short Halo-GAF isoforms (GAF^L and GAF^S) as the sole source. Halo-GAF binds to numerous loci on salivary gland polytene chromosomes, consistent with immunostaining studies^{12,26,27} (**Fig. 1B**), and appears in multiple nuclear foci in diploid circulating larval hemocytes (>90% plasmatocytes, counterpart of mammalian macrophages²⁸), similar to nuclear foci in the S2 cell line²⁹ (**Fig. 1C**). We also constructed transgenic flies expressing C-terminal tagged isoforms GAF^L-Halo and GAF^S-Halo, which exhibit tissue-specific expression²⁶ (**Fig. S1F**) and are functionally active, as indicated by rescue of *Trl*^{13C}/*Trl*^{R67} lethal alleles³. Together, the data demonstrate that fusion of HaloTag does not interfere with the localization and essential functions of GAF.

We investigated the live-cell dynamics of tagged GAF species in live hemocytes (**Fig. S2A**) by SPT, using a ‘fast-tracking’ regime (10 ms/frame) in dSTORM mode³⁰⁻³² to measure slow- and fast-diffusing molecules (**Fig. 1D** and **Movie S1**), and quantified diffusion coefficients with a robust, displacement-based, analytical protocol (Spot-On)³³ (**Fig. 1E** and **Fig. S2B**). All Halo-tagged GAF versions display similar slow and fast diffusivities that are within similar dynamic range demonstrated by histone H2B (**Fig. 1E** and **Fig. S2C**), with >75% and >85% slow-diffusing fraction (chromatin-bound, F_{bound}), respectively. The diffusion coefficient (D) of the bound fraction (D_{bound} 0.004-0.005 $\mu\text{m}^2/\text{s}$) is two orders of magnitude lower than the free fraction (D_{free} 0.75-0.8 $\mu\text{m}^2/\text{s}$) (**Fig. S2E-F**).

A ‘slow-tracking’ regime (500 ms/frame) to motion-blur fast particles allowed selective detection of long- and short-lived chromatin-bound populations (**Fig. S3A-C** and **Movie S2**). We calculated 1-CDF of dwell times to generate survival curves demonstrating apparent GAF dissociation over time. Halo-GAF and GAF^L-Halo show similar profiles, with slightly faster decay for the GAF^S-Halo isoform (**Fig. S3D**). Fitting to a double exponential function (**Fig. S3E**) enabled calculation of long-

and short-lived (called stable and transient) binding fractions, f_{sb} and f_{tb} , and average stable and transient residence times, τ_{sb} and τ_{tb} , after correction for photobleaching and out-of-focus chromatin motions using the apparent dissociation of Halo-H2B as an ‘nondissociative’ standard within the experimental timescale of several minutes (**Fig. S3D**). The stable binding fraction f_{sb} multiplied by total binding fraction F_{bound} gives the overall stable-binding fraction F_{sb} = 30-35 % (**Fig. 1F** and **S2D**). All stable-binding GAF fractions display strikingly protracted residence times τ_{sb} : 130 s for Halo-GAF, 141 s for GAF^L-Halo, and 85 s for GAF^S-Halo, which is 20- to 30-fold longer than the transient residence time τ_{tb} of ~4 s (**Fig. 1G** and **Fig. S3F**), and longer than τ_{sb} values measured for many mammalian transcription factors^{32,34–38}. Stable- and transient-binding are assumed to occur at cognate and non-specific sites, respectively.

POZ, Q-rich, and DBD domains of GAF contribute to stable chromatin binding

Purified, bacterially expressed GAF associates in oligomeric complexes ranging from monomers to multimers^{39,40}, and GAF complexes are also observed in nuclear extracts of S2 cells. Multimerization is mediated by the POZ and Q-rich domains of GAF^{39–41}. To investigate how GAF domains contribute to particle dynamics, we used CRISPR-Cas9 to engineer Halo-GAF deletions in the POZ domain (ΔPOZ), the zinc finger (ZF^9 ; ZF^{10}), and the long and short Q-rich domains (ΔQ) (**Fig. 2A** and **Fig. S4A-E**).

Homozygous ΔPOZ and ZF^9 or ZF^{10} mutants arrest at early pupal and early 3rd instar larval stages, respectively, while homozygous ΔQ is 70% viable, producing infertile adults with impaired longevity (**Fig. 2A**). These manifest phenotypes, although late in development owing to perdurance of the untagged WT GAF contributed by the heterozygous mother to homozygous oocytes, indicate that all three GAF domains are essential for *Drosophila* viability.

SPT using fast and slow tracking regimes for Halo-GAF ΔPOZ , ZF^9 , ZF^{10} and ΔQ mutants in 3rd instar larval hemocytes found that all three domain mutants display substantial reductions in F_{sb} and τ_{sb} for the slow-diffusing fraction (**Fig. 2B-C** and **Fig. S5A-C**). Disruption of the POZ domain reduces F_{sb} from 29% to 15%, and τ_{sb} from 130 s to 42 s, demonstrating the important contribution of this multimerization domain to stable chromatin association. Deletion of Q-rich domains shows a modest reduction of F_{sb} from 29% to 24%, and reduces the τ_{sb} from 130 s to 49 s. Interestingly, under fast-tracking, ΔPOZ and ΔQ proteins exhibit similar D_{free} but larger D_{bound} compared to WT GAF, suggesting a more diffusive binding mode (**Fig. S5D-E**). These results are consistent with the specific binding patterns of ΔPOZ and ΔQ on fixed polytene chromosomes (**Fig. 2D**)

The zinc finger mutants ZF^9 and ZF^{10} also show reductions in F_{sb} to 19% and 22%, and τ_{sb} to ~40 s in hemocytes (**Fig. 2B-C** and **Fig. S5A-C**), similar to ΔPOZ and ΔQ . However, unlike ΔPOZ and ΔQ , both ZF^9 and ZF^{10} mutants exhibit loss of the specific binding pattern on polytene chromosomes and increase of nucleoplasmic distribution (**Fig. 2D**). These results confirm the crucial function of the DNA-binding zinc finger for site-specific chromatin binding, and report aberrant, mechanistically unclear diffusive behavior of ZF^9 and ZF^{10} mutant proteins. Notably, the time-averaged Mean Squared Displacement (MSD) curves from slow-tracking of ZF^9 and ZF^{10} show an

initial steep rise followed by a plateau after 10 s, a profile dramatically different from *WT* GAF, Δ POZ, Δ Q, and H2B HaloTag fusions, all of which display a linear or Brownian increase of the MSD over a 60 s timescale (**Fig. S5F**).

Chromatin binding kinetics by GAF is independent of recruited remodelers NURF and PBAP

At cognate GAGAG sites on *Drosophila* chromatin, GAF recruits NURF and PBAP, ATP-dependent chromatin remodelers of the ISWI and SWI/SNF families, respectively, to drive DNA accessibility for neighboring transcription factors and establish promoter-proximal paused Pol II^{13,17,19,24,42,43}. This process begins during *Drosophila* embryogenesis, when GAF and the Zelda pioneer factor are individually required to activate and remodel the chromatin accessibility landscape for widespread zygotic transcription^{25,29}. However, it was unclear whether the recruitment of NURF and PBAP by GAF is required to assist its own chromatin binding as a pioneer factor. To address this, we performed SPT of GAF^L-Halo and GAF^S-Halo on 3rd instar larval hemocytes isolated from *bap170* and *nurf301/E(bx)* mutants for unique subunits in PBAP^{43,44} and NURF^{19,43} complexes, respectively (**Fig. 3A**). The results show little or small changes in the F_{bound} , D_{bound} and τ_{sb} values of the mutants (**Fig. 3B-C** and **Fig. S6A-F**). GAF^L-Halo and GAF^S-Halo isoforms also show no qualitative global binding changes on polytene chromosomes in the *bap170* and *nurf301* mutants, although changes in a minority of chromosomal loci might escape detection (**Fig. 3D**). (By contrast, changes of HSF-Halo binding can be detected in mutants; see below). These findings are generally consistent with ChIP-Seq studies showing similar average GAF binding genome-wide in PBAP-depleted S2 cells (**Fig. S7**), although partial GAF binding is observed in a subset of *Drosophila* promoters (685 promoters displaying reductions in paused RNA Pol II and chromatin accessibility)²⁴. Taken together, our live-cell SPT results indicate that GAF chromatin binding and dwell time are largely autonomous from NURF and PBAP, although other remodeling activities are not excluded⁴⁵. We conclude that the main beneficiaries of NURF and PBAF recruitment and nucleosome remodeling activities are GAF's 'non-pioneer' neighbors.

Heat shock increases chromatin-binding fraction of HSF without affecting dwell time

The recruitment of chromatin remodelers by GAF increases accessibility to facilitate binding of Heat Shock Factor (HSF) to the tripartite Heat Shock Element (HSE) adjacent to GAF binding sites at heat shock promoters^{18,46-49}. Under normal conditions, HSF is predominantly monomeric, with low (submicromolar) affinity of its winged-helix DBD for an NGAAN sequence^{50,51}; heat shock induces HSF trimerization and juxtaposition of three DBDs for high-affinity binding to HSEs containing triple NGAAN sequences in alternating orientation⁵²⁻⁵⁷.

To measure HSF dynamics, we constructed a transgenic HSF-Halo strain under natural expression control, and verified the functionality of HSF-Halo by rescue of *P{PZ}Hsf⁰³⁰⁹¹/Hsf³* lethal alleles^{58,59}. We further validated HSF-Halo functions by confocal imaging of fixed polytene nuclei, which showed that HSF-Halo is mostly nucleoplasmic at room temperature (RT), except for low binding to few sites including *Hsp83* harboring very high affinity HSEs; heat shock at 37.5 °C for 10 or 30 min induced strong HSF binding to many more chromosomal loci, most prominently reported at

Hsp genes^{52,60} (**Fig. S8A**). This inducible pattern of HSF binding on heat shock is partially reduced in mutants for *Trl*, *Bap170* and *Nurf301* (**Fig. S8A**). (Note that there are GAF-independent HSF targets in the genome¹⁸, for which changes of HSF binding at corresponding polytene loci would not be expected). Imaging of fixed hemocytes shows that the heterogeneous distribution of HSF-Halo changes on heat shock to a more punctate pattern including several prominent foci, consistent with previous studies (**Fig. 4A**)^{52,61,62}.

We performed live-cell SPT on HSF-Halo in fast- and slow-tracking modes in the $P\{PZ\}Hsf^{03091}/Hsf^3$ genetic background, using hemocytes cultured at RT or heat shocked at 37.5 °C (**Fig. 4B**). As expected, the overall binding F_{bound} of HSF from fast-tracking increases substantially from 24.9% to 44.3% upon heat shock (**Fig. 4C** and **Fig. S8B**). Importantly, two-component exponential decay fitting of the HSF-Halo survival curves derived from slow tracking reveals a substantial increase of stable binding F_{sb} from 5.9% to 14.2% upon heat shock with no measurable change of residence time τ_{sb} (47s) (**Fig. 4C-D** and **Fig. S8C, E**). Thus, heat shock elevates the stable chromatin-binding HSF trimer fraction without affecting the dissociation rate (inverse of residence time), and suggests that the limited stable binding at RT ($F_{\text{sb}} = 5.9\%$) is due to low-level trimerization⁵⁷. Distinct from HSF dynamics, GAF shows a small overall reduction in F_{bound} on heat shock (from 77.3% to 69.6%), and similarly for the stable binding fraction F_{sb} (from 29.4% to 22.1%) (**Fig. 4C**). Importantly, the residence time τ_{sb} for GAF remains unchanged after heat shock (**Fig. 4D** and **S8D-E**).

Chromatin-bound GAF displays H2B-like confinement

The diffusion coefficient of chromatin-bound HSF measured by fast-tracking (D_{bound} , average of both stable- and transient-binding) at RT where HSF monomers predominate is ~4-fold greater than that of HSF trimers induced by heat shock ($D_{\text{bound}} = 0.075$ vs $0.019 \text{ } \mu\text{m}^2/\text{s}$) (**Fig. 4E**). HSF monomers also exhibit >10-fold larger D_{bound} values than GAF ($D_{\text{bound}} = 0.0046 \text{ } \mu\text{m}^2/\text{s}$) (**Fig. 4E**), indicating that a single DBD is more diffusive on chromatin than multiple DBDs. Intriguingly, D_{bound} for GAF approaches the H2B value ($D_{\text{bound}} = 0.0020 \text{ } \mu\text{m}^2/\text{s}$) (**Fig. 4E**). To strengthen these findings, we analyzed particle trajectories with vbSPT, a variational Bayesian Hidden Markov Model (HMM) algorithm that assigns bound and free diffusive states to individual particle displacements of each trajectory^{63,64} (**Fig. S9A-B**). We classified particle trajectories as either ‘bound’ or ‘free’, excluding a small fraction showing two-state diffusivity (**Fig. S9A-D**). The time-averaged MSD plots of the bound particles confirm that bound molecules move in small confined regions (**Fig. 4F** and **Fig. S10A**), while free molecules undergo Brownian motion (**Fig. S10B**). The MSD plot of chromatin-bound GAF trajectories reaches a plateau at low values, resembling that of H2B (**Fig. S10A**), while HSF plateaus at higher values (**Fig. 4F**). The radius of confinement (R_c) gives median values for HSF monomers ($0.13 \text{ } \mu\text{m}$), HSF trimers ($0.10 \text{ } \mu\text{m}$), GAF multimers ($0.07 \text{ } \mu\text{m}$), and H2B ($0.06 \text{ } \mu\text{m}$) (**Fig. S10C**). Together, the results indicate that chromatin-bound GAF is nearly as constrained as nucleosomal histones. Activated HSF trimers are less constrained than GAF, possibly due to fewer DBDs per complex and/or higher local chromatin mobility, but bound HSF monomers are more diffusive, consistent with the presence of only a single DBD.

Constitutively high temporal occupancy defines pioneering activity

The steady-state open chromatin landscape at promoters and enhancers featuring nucleosome-depleted regions genome-wide^{45,65,66} belies highly dynamic interactions with transcription and chromatin factors⁶⁷⁻⁷². The establishment and maintenance of chromatin accessibility, i.e. the sustained opening of chromatin, requires the joint activities of sequence-specific DNA-binding factors and ATP-dependent remodeling enzymes^{12,19,24,25,73,74}, the latter proteins interacting with chromatin with a lifetime of seconds^{67,69,70}. GAF directs pioneering functions not only by virtue of its affinity for nucleosomal DNA targets^{12,75} but also recruitment of chromatin remodelers^{12,14,15,24,42,76}. Given the highly transient association and variable occupancy levels displayed by remodelers^{67,70}, we hypothesized that GAF should instead sustain high occupancy along with protracted dwell time to continuously maintain open chromatin at cognate targets .

Temporal occupancy, the percent time of any duration for which a cognate site is factor-bound, depends on the number of GAF molecules ($N_{\text{molecules}}$) per cell and the number of target sites (N_{sites}) in the genome. In the context of the facilitated diffusion model⁷⁷ in which transcription factors experience 3D nucleoplasmic diffusion, nonspecific binding, 1D diffusion, dissociation and re-binding until site-specific chromatin engagement, temporal occupancy is also dependent on the kinetics of target search and dissociation. Integration of our kinetic data from SPT with published genomic data allows calculation of temporal occupancy for GAF.

ChIP-seq identifies 3622 high-confidence GAF peaks from the hemocyte-like S2 cell line^{17,78,79}. Similar numbers of GAF peaks are found by ChIP-seq analysis of larval imaginal tissues and embryos although the peaks from different cell types overlap partially^{25,80}. We measured GAF abundance by fluorescence flow cytometry using a calibrated CTCF standard⁸¹, estimating $N_{\text{molecules}} = 56,683 \pm 6,025$ GAF molecules per hemocyte (**Fig. S11A**). Given that circulating hemocytes are largely in the G2 cell cycle phase (**Fig. S11B-C**), we estimate $N_{\text{sites}} = 3622 \times 4$ genome copies = 14,488. From the overall chromatin-binding fraction [F_{sb}], residence times and fractions for stable and transient chromatin-binding (τ_{sb} , f_{sb} , τ_{tb} , f_{tb}), we derived the average search time ($\tau_{\text{search}} = 150$ s, the time from GAF dissociation from one stable target to association with the next) and the sampling interval (SI = 71.5 s, the time from the start of one stable-binding event to the next stable event on the same chromatin target; see methods), assuming that GAF binds stably at specific sites and transiently elsewhere (**Fig 5A-B**).

We calculated the average occupancy to be 182% for a GAF peak from values of SI and τ_{sb} (occupancy = $\tau_{\text{sb}}/\text{SI}$), while the occupancies for ΔPOZ ($N_{\text{molecules}} = 44,907 \pm 14,154$) and ΔQ ($N_{\text{molecules}} = 66,206 \pm 3,064$) drop strikingly to 17% and 32%, assuming the same number of targets (**Fig. 5B**). This 182% occupancy is averaged over the 3622 GAF peaks whose intensities are correlated with increasing numbers of GAGAG elements. Notably, ~65% of GAF peaks harbor more than two non-overlapping GAGAG elements, with median peak intensity rising to a plateau at 6-7 clustered elements¹⁷(**Fig. 5C**), e.g. at *ubx*, *engrailed*, *E74*, *eve*, and *Hsp* genes⁴. The results indicate that GAF binds at least as a dimer on average, with a distribution tending towards larger oligomers for peaks showing high ChIP-seq signals, which can be attributed to the cooperative

binding of GAF, as demonstrated *in vitro*^{39,40}. At this subset of highly-enriched sites, GAF may bind as a multimeric complex with essentially full temporal occupancy despite factor on-off dynamics (**Fig. 6**) for a time period of any duration in which GAF levels and the number of GAF targets remain unchanged.

We note that many GAF-binding peaks overlap with Pipsqueak, a related POZ-domain transcription factor^{82,83} and partially with CLAMP, another GA repeat-binding pioneer factor in *Drosophila*^{84,85}. The overall site occupancy at GAF locations on chromatin is therefore likely to be further supplemented when the contributions of Pipsqueak and CLAMP are quantified.

For HSF, we determined $N_{\text{molecules}} = 9,543 \pm 613$ for a sole source, transgenic HSF-Halo under natural expression control in the $P\{PZ\}Hsf^{03091}/Hsf^3$ background (**Fig. S11A**). A similar calculation for HSF-Halo binding to 442 genomic sites after heat shock⁴⁸ gives $\tau_{\text{search}} = 119$ s, and $SI = 31$, which results in an average HSF occupancy of 153%, or 51% for HSF trimers as the predominant species induced after 10-40 min heat shock (**Fig. 5B**). At highly-enriched HSF locations such as the major *Hsp* genes harboring several HSEs, it follows that one or more HSF trimers may occupy the promoter 100% of the time on full induction to release the paused RNA Pol II and rapidly recruit additional enzymes for a burst of transcription until system attenuation (**Fig. 6**).

Discussion

Full complement of GAF domains promote kinetics of stable chromatin association

Our single-particle tracking of GAF in live hemocytes reveals that GAF binds chromatin with an exceptionally long residence time τ_{sb} of ~ 2 min compared to other factors. Systematic mutagenesis showing that the DBD, the POZ multimerization domain and the Q-rich domains are required for viability also found that not just the DNA-binding Zinc finger, but all three GAF domains are required for its stable chromatin association and long τ_{sb} (**Fig. 2B-C**). Of interest, the Zinc finger mutants ZF^9 and ZF^{10} have a substantial residual slow-diffusing fraction in hemocytes, but show no specific binding on polytene chromosome bands (**Fig. 2B, D**). This is possibly due to non-specific association of the altered zinc finger and the remaining basic regions of the DBD (**Fig. 2A and Fig. S4**), and/or protein-protein interactions of the intact POZ or Q-rich IDR domains (intrinsically disordered regions). Overall, our findings are consistent with the contributions to specific and non-specific DNA binding shown by mutant DBDs of mammalian TFs^{32,36,86}, and with the observation of IDR-assisted, *in vivo* DNA binding specificity for two yeast TFs⁸⁷. Of note, mutant GAF proteins ZF^9 and ZF^{10} also exhibit an aberrant, slow-diffusing species whose underlying mechanism is unknown and remains to be further explored (**Fig. S5F**).

The POZ domain is found at the N-terminus of vertebrate and invertebrate transcriptional regulators implicated in development and disease⁸⁸. Functionally, the POZ domain is involved in protein homo- and hetero-dimerization, as well as multimerization⁸⁸. The POZ domain mediates multimerization of GAF, which facilitates cooperative binding to closely clustered GAGAG

elements^{39,40}, and assists long-distance promoter-enhancer interactions between well-separated GAGAG clusters⁸⁹. As judged by the kinetic behaviors of the GAF POZ mutant, we conclude that multimerization of GAF constitutes a critical element for its ability to pioneer open chromatin. Similarly, a variant glucocorticoid receptor (GR) that mimics allosterically induced GR tetramerization converts GR to a super-receptor that enhances chromatin occupancy at normally inaccessible sites⁹⁰.

Autonomy from recruited chromatin remodelers

The coupling of GAF-mediated pioneering of chromatin accessibility to ATP-dependent chromatin remodeling activities has been reported from the outset of studies on the mechanism underlying DNase hypersensitive sites¹². Biochemical experiments have since demonstrated that GAF directly recruits remodelers NURF and PBAP via protein-protein interactions, in addition to a number of other chromatin-based factors⁷⁶. Using mutants for NURF and PBAP, we now show that their recruitment is not obligatory for GAF to kinetically engage chromatin targets. This indicates that GAF is largely autonomous from recruited remodelers and that the ensuing chromatin remodeling to antagonize competing processes of nucleosome encroachment primarily benefits the binding or activity of neighboring TFs to chromatin targets. While other factors or the global background of remodeling activities are not excluded from modulating GAF binding, GAF's relative autonomy from two prominent recruited members of the SWI/SNF and ISWI remodeler families at the initial step of chromatin association may define an important property of transcription factors that act as pioneering agents.

High constitutive and inducible temporal occupancies by GAF and HSF

By curating genomic databases for the number of genomic targets and integrating these parameters with measured kinetics and abundance, we found that GAF binds to its target sites with temporal occupancy of 182% for 3622 high-confidence ChIP-seq peaks¹⁷ (**Fig. 5A-C**), i.e. with near full occupancy as a dimer on average. For genomic sites with greater than average GAF ChIP enrichment and number of GAGAG elements (**Fig. 5B**), this occupancy is likely to involve higher oligomers, consistent with the native biochemical states of GAF complexes. Such high occupancy, or kinetic persistence, whereby factor dissociation from chromatin and replacement are essentially simultaneous, maintains a constant barrier and magnet for remodeler recruitment at GAF targets. (GAF multimers appear as stable biochemical complexes^{39,40}, but dynamic exchange of GAF monomers within a multimeric complex is possible in principle and awaits further study). We envision that a substantial fraction of GAF targets in the genome displays high oligomeric status and temporal occupancy (~100%), while the remaining targets showing progressively lower occupancies, consistent with the genome-wide continua of transcription factor binding levels on metazoan genomes that reflect functional, quasi-functional, and nonfunctional transcription control^{91,92}.

Unlike GAF, HSF monomers under room temperature conditions inducibly trimerize on heat shock⁵⁷ which significantly increases the chromatin-bound fraction (F_{bound}) without changing

stable residence time (τ_{sb}). For ~ 400 activated HSF-binding sites on the *Drosophila* genome⁴⁸, we estimate an average of $\sim 50\%$ temporal occupancy by one HSF trimer. At the major *Hsp* loci harboring greater than average ChIP-seq signal intensity and multiple HSE elements, we envision that one or more HSF trimers engage at near full (100%) temporal occupancy. Full occupancy by HSF on heat shock induction may be required to facilitate release of the paused RNA Polymerase II previously established by GAF, and to sustain recruitment-release of new transcription pre-initiation complexes for a strong transcriptional burst of HS-responsive genes.

Pioneering of chromatin accessibility is a process involving multiple inputs

The pioneer transcription factor concept has been introduced and elaborated for over two decades with a focus on special nucleosome binding properties of the FoxA1 prototype proposed to initiate establishment of chromatin accessibility for the benefit of consequent binding of neighboring TFs⁹³. However, there continues to be debate whether the reported properties of FoxA1 are sufficiently distinct to set it apart from other transcription factors^{16,35,94,95}. Our early findings on GAF that predate the controversy have documented that nucleosome binding and ATP-dependent remodeling are functionally coupled in a biochemical assay¹², and additional studies to the present - including the genome-wide effects of remodeler depletion on chromatin accessibility²⁴ and nucleosome positioning at GAF targets⁷³ - support the concept that GAF directly recruits remodelers for the site-specific creation of accessible chromatin.

Thus, there is ample evidence to include remodeler recruitment by GAF or other TFs³⁵ as a fundamental biochemical criterion for pioneering besides affinity for nucleosomes or closed chromatin³⁶. Our finding of autonomous remodeler recruitment (chromatin interaction kinetics of GAF being largely unaffected in NURF and PBAP mutants) provides additional insight on the hierarchical nature of pioneering wherein GAF binding to chromatin at the initial stage of pioneering (stage 1) would be followed by remodeler recruitment and ATP-dependent nucleosome mobilization to create DNase hypersensitivity, thereby facilitating assembly of the transcription preinitiation complex (PIC), paused Pol II, and the inducible binding of HSF (stage 2) (**Fig. 6**). In addition to remodeler recruitment, constitutively full temporal occupancy by GAF revealed by the single-particle kinetics provides a quantitative criterion for pioneering long-term chromatin accessibility primed for the transcriptional responses to homeostatic, environmental, and developmental signals.

However, we emphasize that high temporal occupancy is not an obligatory consequence of GAF's long residence time on chromatin, or its multimeric, cooperative binding to GAGAG elements. Occupancy is also dependent on cellular GAF expression, abundance, and the number and genomic distribution of GAGAG elements in *Drosophila*. Thus, it may be instructive to consider pioneering as an active process with the multiple inputs we have described - autonomous factor-binding to closed chromatin, remodeler recruitment, nucleosome mobilization, and for the subset of transcription factors that maintain accessible chromatin constitutively, correspondingly high temporal occupancy, not excluding additional criteria to be identified. We hope that inclusion of these biochemical and kinetic principles guides further investigations on the

substantial fraction of computationally identified human TFs (16% of ~700 TFs)¹⁶ that may pioneer chromatin accessibility as a basic mechanism of genome regulation in eukaryotic organisms.

FIGURE LEGENDS

Figure 1

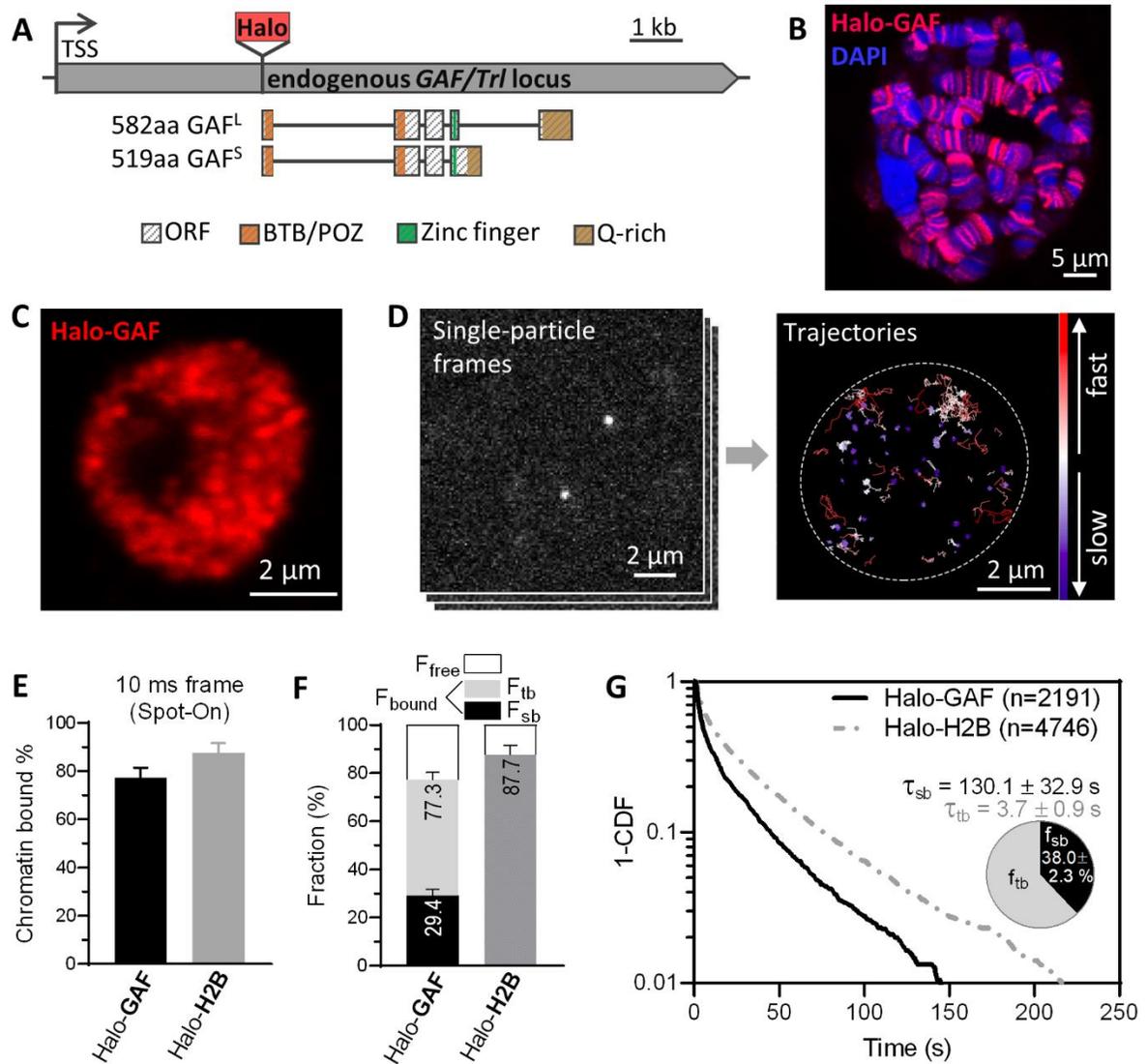


Figure 1. Chromatin-binding dynamics of GAF shown by single-particle tracking (SPT) in live *Drosophila* hemocytes.

- (A) Diagram of HaloTag (Halo) knock-in at the N-terminus of endogenous *GAF/Trl* locus. Protein domains in color. TSS, transcription start site. C-terminal GAF-HaloTag fusions for two splicing isoforms GAF^S (short) and GAF^L (long) are shown in Fig S1.
- (B) Halo-GAF binds to specific polytene chromosome loci in fixed 3rd instar larval salivary gland nuclei, revealed by JF552 fluorescence (red); DNA counterstained with DAPI (blue).
- (C) Confocal distribution of Halo-GAF (JF552) foci in fixed 3rd instar larval hemocyte nuclei (predominantly diploid plasmatocytes in G2 phase of the cell cycle).
- (D) SMT frames and superimposed trajectories of Halo-GAF in live hemocytes, color-coded according to diffusion coefficients. Dashed oval marks the nucleus.
- (E) Spot-On kinetic modeling of fast-tracking data shows chromatin-bound and free fractions for Halo-GAF and Halo-H2B. Results are mean \pm SD from three biological replicates.
- (F) Chromatin-free fraction (F_{free}), global stable- and transient-binding fractions (F_{sb} and F_{tb}) of Halo-GAF extracted from fast- and slow-tracking data in (E) and (G), with error propagation.
- (G) Survival probability curves (1-CDF) plotted from apparent dwell times of thousands (n) of single-particle chromatin-binding events for Halo-GAF. Average residence times for stable- (τ_{sb}) and transient- (τ_{tb}) binding by Halo-GAF are corrected by using Halo-H2B as a 'non-dissociating' standard. Pie charts show stable- (f_{sb}) and transient-binding (f_{tb}) fractions. Mean and SD provided. Errors represent bootstrapped SD.

Figure 2

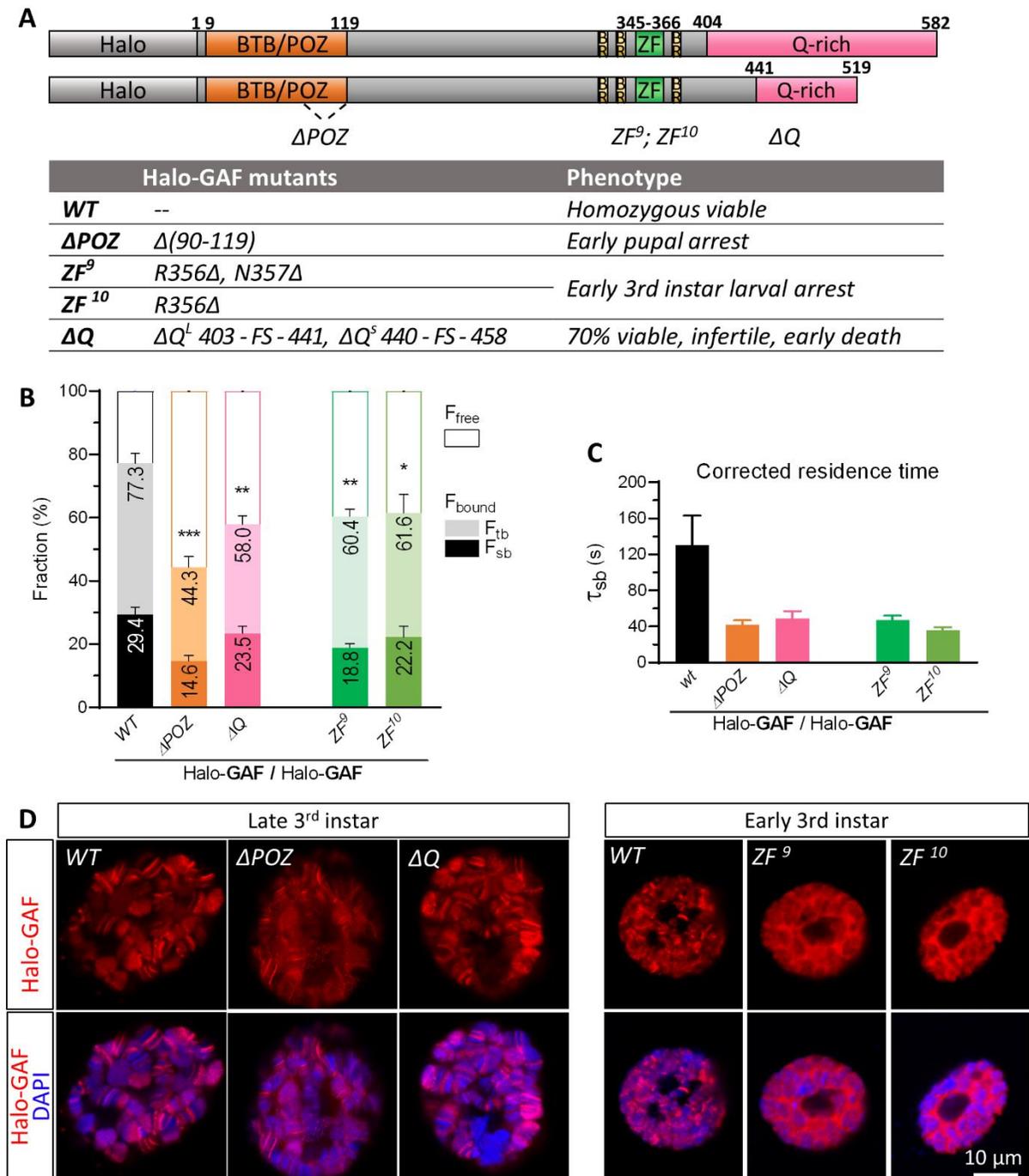


Figure 2. POZ, Q-rich, and DBD domains of GAF all contribute to stable chromatin binding and long residence times.

- (A) Schematics of Halo-GAF^L (long) and Halo-GAF^S (short) isoforms with functional domains to scale. BTB/POZ: Broad-complex, Tramtrack and Bric-à-brac/Poxvirus and Zinc finger, BR: basic region, ZF: zinc finger, Q-rich: glutamine-rich. Halo-GAF deletions were generated by CRISPR-Cas9. Δ POZ contains a 90bp deletion in the second exon, generating a 30-AA deletion (Δ 90-119) of the POZ domain, which includes G93 and L112 that are essential for transcription activation²⁹. The deleted Arg and Asn amino acids in the zinc finger (ZF^9 , ZF^{10}) make contact with 'GAG' of the consensus GAF binding site(Omichinski et al. 1997). Δ Q contains small deletions at the beginning of Q-rich domains of both long and short isoforms, resulting in frame shift and truncation of Q-rich domains. Table reports mutant phenotypes. FS: frameshift.
- (B) Global chromatin-bound and free fractions (%) for wild type (*WT*) and mutant Halo-GAF. Fast and slow tracking results with propagated errors.
- (C) Average residence times for *WT* and mutant Halo-GAF, corrected as in Fig. 1. Error bars represent bootstrapped SD.
- (D) Halo-GAF distribution on fixed salivary gland (SG) polytene nuclei for *WT* and GAF mutants. Δ POZ and Δ Q nuclei are from late 3rd instar larvae with *WT* nuclei from the same stage as control. ZF^9 and ZF^{10} polytene nuclei are from early instar larvae with *WT* nuclei from the same stage as control. Red: Halo-GAF; blue: DAPI. One representative confocal z-section is shown.

Figure 3

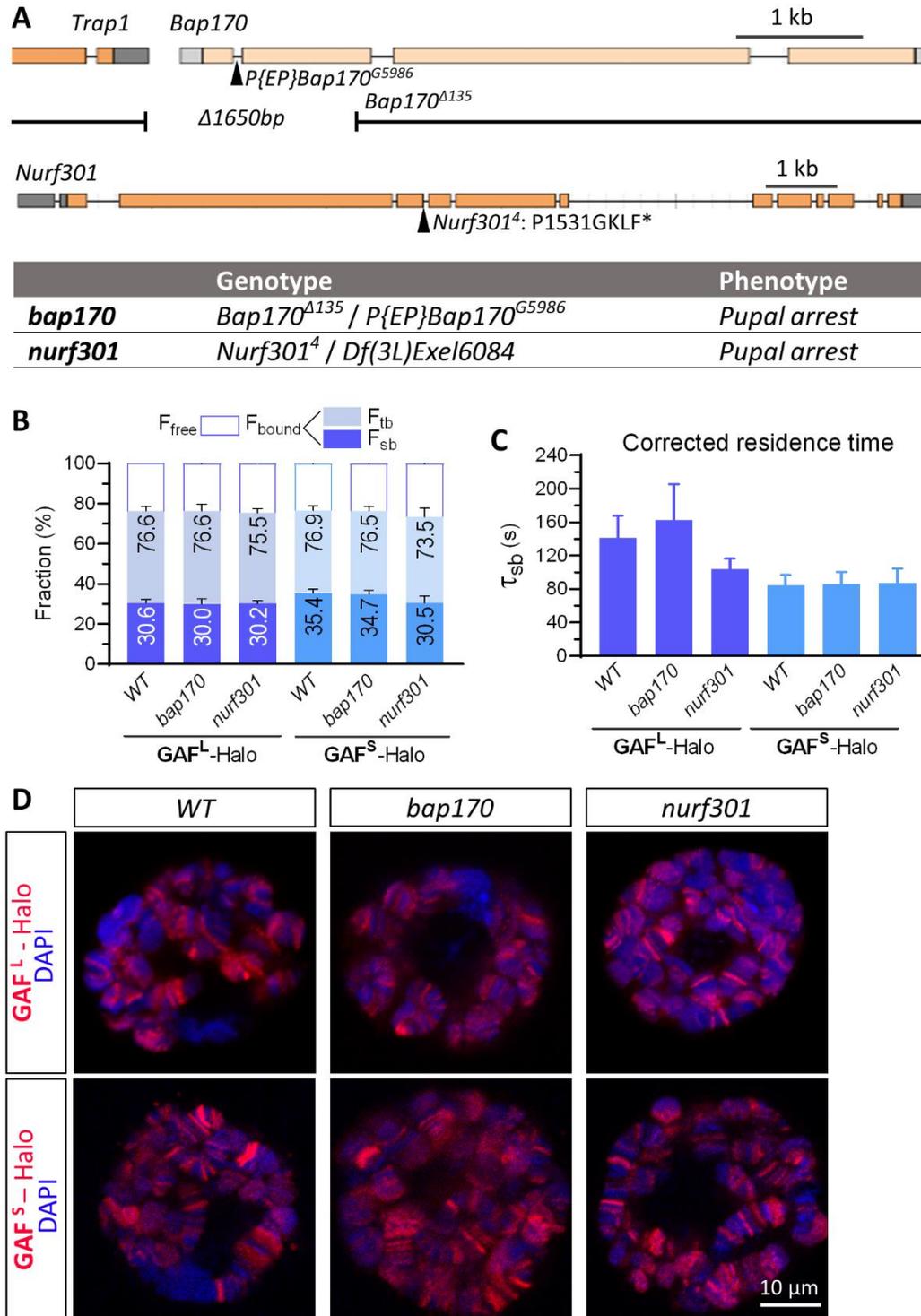


Figure 3. Chromatin binding by GAF is largely independent of remodelers PBAP and NURF.

- (A) *Bap170* and *Nurf301/E(bx)* mutants and phenotypes. *Bap170*^{Δ135} harbors a 1650bp deletion spanning the promoter, 5'UTR and first two exons of *Bap170*, *P{EP}Bap170*^{G5986} has a *P{EP}* element insertion at 447 bp downstream from the transcription start site in the first intron of the gene. *Bap170*^{Δ135} abolishes *Bap170* expression and strongly reduces polybromo protein level at larval stage, causing pupal lethality when homozygous (Carrera et al. 2008), while flies homozygous for the *P{EP}Bap170*^{G5986} die primarily as pharate adults, with only 3% male homozygous adults (Chalkley et al. 2008). Transheterozygous *Bap170*^{Δ135}/*P{EP}Bap170*^{G5986} (denoted as *bap170*) also exhibits pupal arrest. *Nurf301*⁴ contains a splice-donor site mutation that blocks splicing of the fourth intron. The aberrant transcript introduces four additional amino acids (GKLF) and an in-frame stop codon after P1531, truncating C-terminal 609-1230 aa including the essential PHD finger and Bromodomain (Badenhorst et al. 2002). *Nurf301*⁴ is pupal-lethal with <60% pupariation rate (Badenhorst et al. 2005). When transheterozygous with a deletion allele spanning 31 genes including *Nurf301*, *Nurf301*⁴/*Df(3L)Exel6084* (denoted as *nurf301*) also shows pupal arrest.
- (B) Global chromatin-bound fractions for GAF^L-Halo and GAF^S-Halo in wild type (*WT*), *bap170* and *nurf301* mutants. Fast and slow tracking results with propagated errors. All three strains express transgenic GAF^L-Halo or GAF^S-Halo under natural regulation, in the presence of endogenous, untagged GAF. See methods for genotypes of *WT*, *bap170*, and *nurf301*.
- (C) Corrected average residence times for GAF^L-Halo and GAF^S-Halo in *WT*, *bap170* and *nurf301* mutants. Error bars represent bootstrapped SD.
- (D) GAF^L-Halo and GAF^S-Halo distributions on fixed salivary gland polytene nuclei for *WT*, *bap170* and *nurf301* mutants.

Figure 4

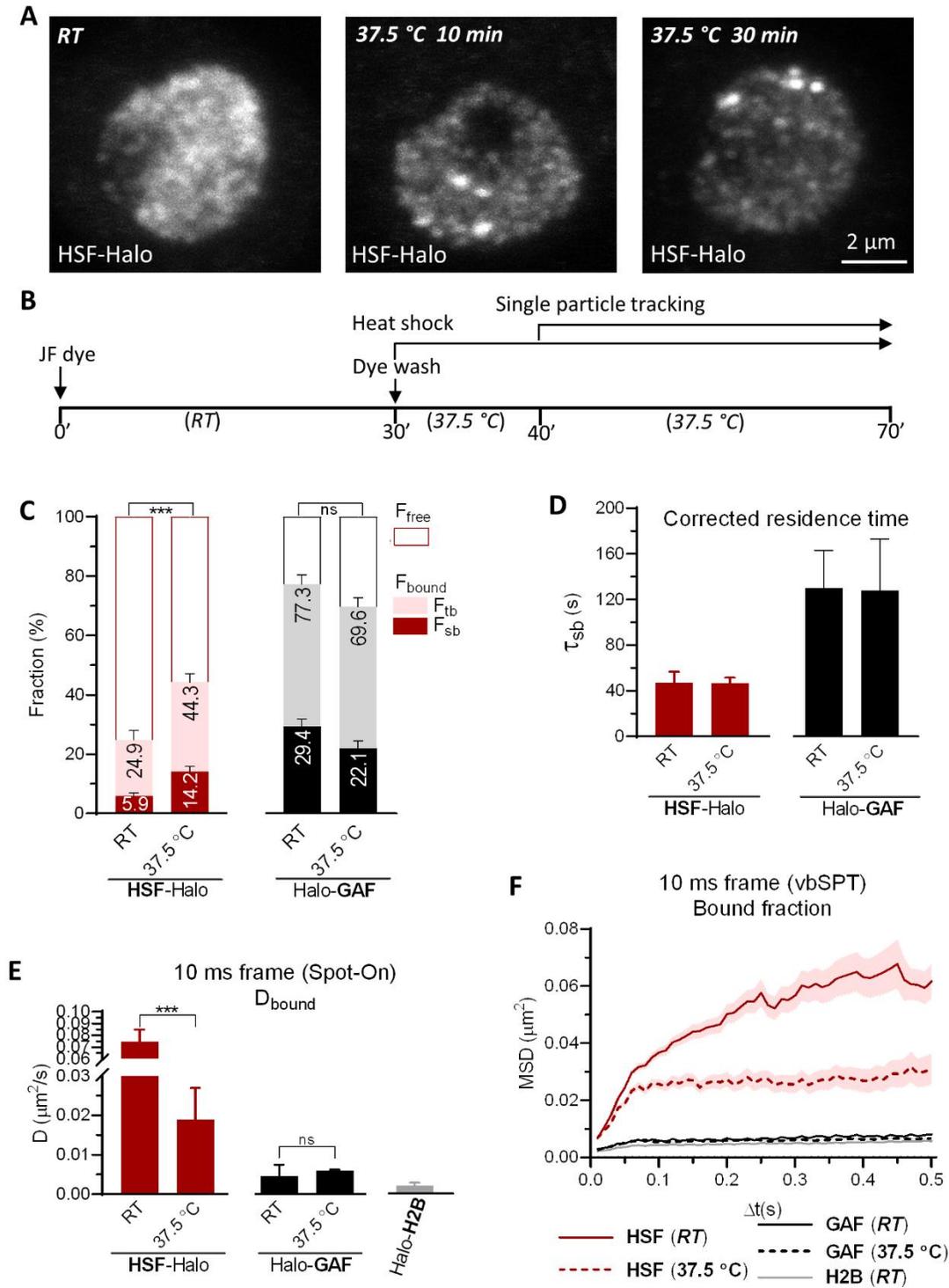


Figure 4. Heat shock increases chromatin binding fraction of HSF without affecting dwell time

- (A) Maximum-intensity z-stack projection of HSF-Halo in fixed hemocytes. HSF-Halo forms several prominent foci upon heat shock at 37.5°C. Maximum projections of confocal z-stacks are shown.
- (B) Flow chart of the heat shock and live-hemocyte imaging procedure. SPT starts 10 min after heat shock and continues over multiple cells (1-2 min per cell) for a total of 30 min with each sample.
- (C) Global chromatin-bound fractions for HSF-Halo and Halo-GAF at room temperature (*RT*) and 37.5°C. Fast and slow tracking results with propagated errors.
- (D) Corrected average residence times for HSF-Halo and Halo-GAF at *RT* and 37.5°C. Error bars represent bootstrapped SD.
- (E) Diffusion coefficients derived using Spot-On for bound fractions of HSF-Halo and Halo-GAF at *RT* and 37.5°C, and Halo-H2B at *RT*.
- (F) Average MSD versus lag time of bound trajectories classified by vbSPT for HSF-Halo, Halo-GAF and Halo-H2B at *RT* and 37.5°C, and Halo-H2B at *RT*. See Fig. S10A for a zoomed-in section for GAF and H2B.

Figure 5

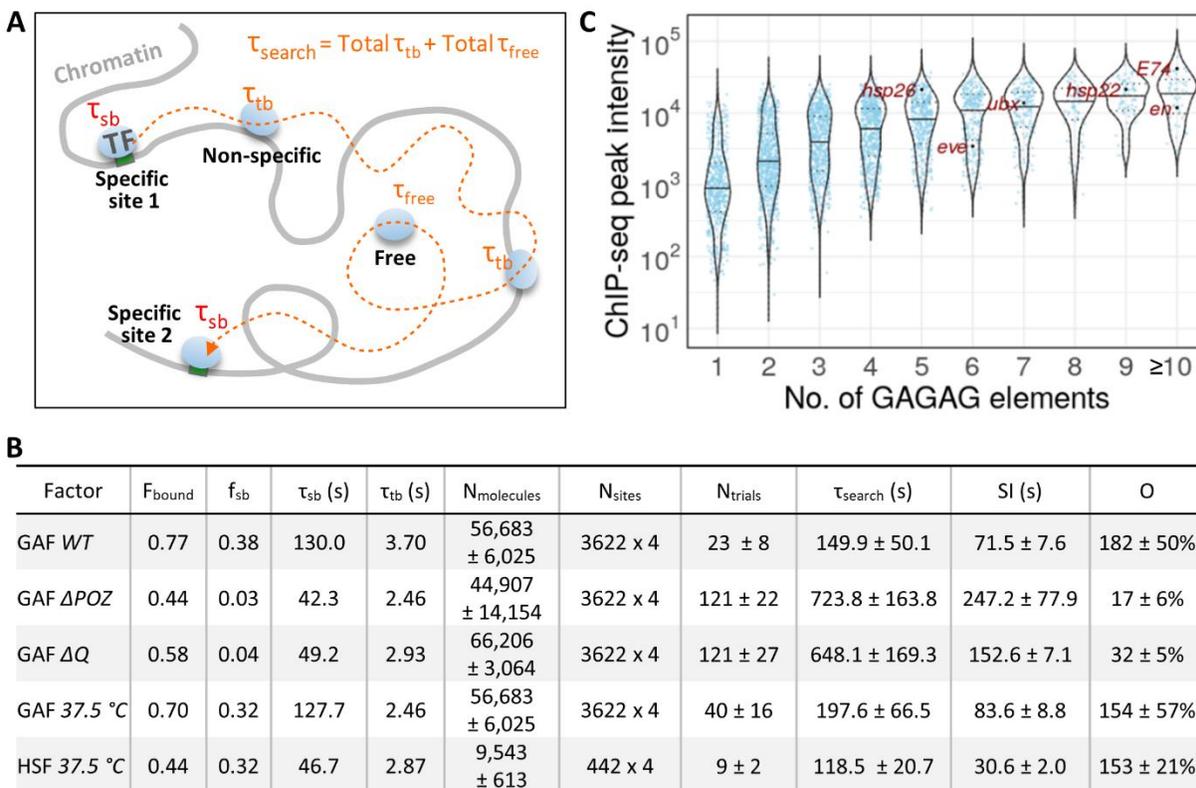


Figure 5. High site occupancy and remodeler autonomy quantifies pioneering criteria

- (A) Schematic of a TF trajectory between two specific chromatin targets showing the search time τ_{search} , stable τ_{sb} and transient τ_{tb} dwell times, and τ_{free} . The TF molecule dissociates from a specific target, and samples nonspecific sites for a number of trials before encountering the next specific target. The τ_{search} equation is indicated (see methods).
- (B) Violin plots of GAF ChIP-seq peak intensities (analysis of S3 Table from Fuda et al, 2015) in hemocyte-like S2 cells plotted by the number of non-overlapping GAGAG elements identified with HOMER⁹⁶.
- (C) Key SPT and $N_{\text{molecules}}$ parameters measured in this study and N_{sites} from the literature^{17,48} are used to calculate occupancy levels for GAF and HSF.

Figure 6

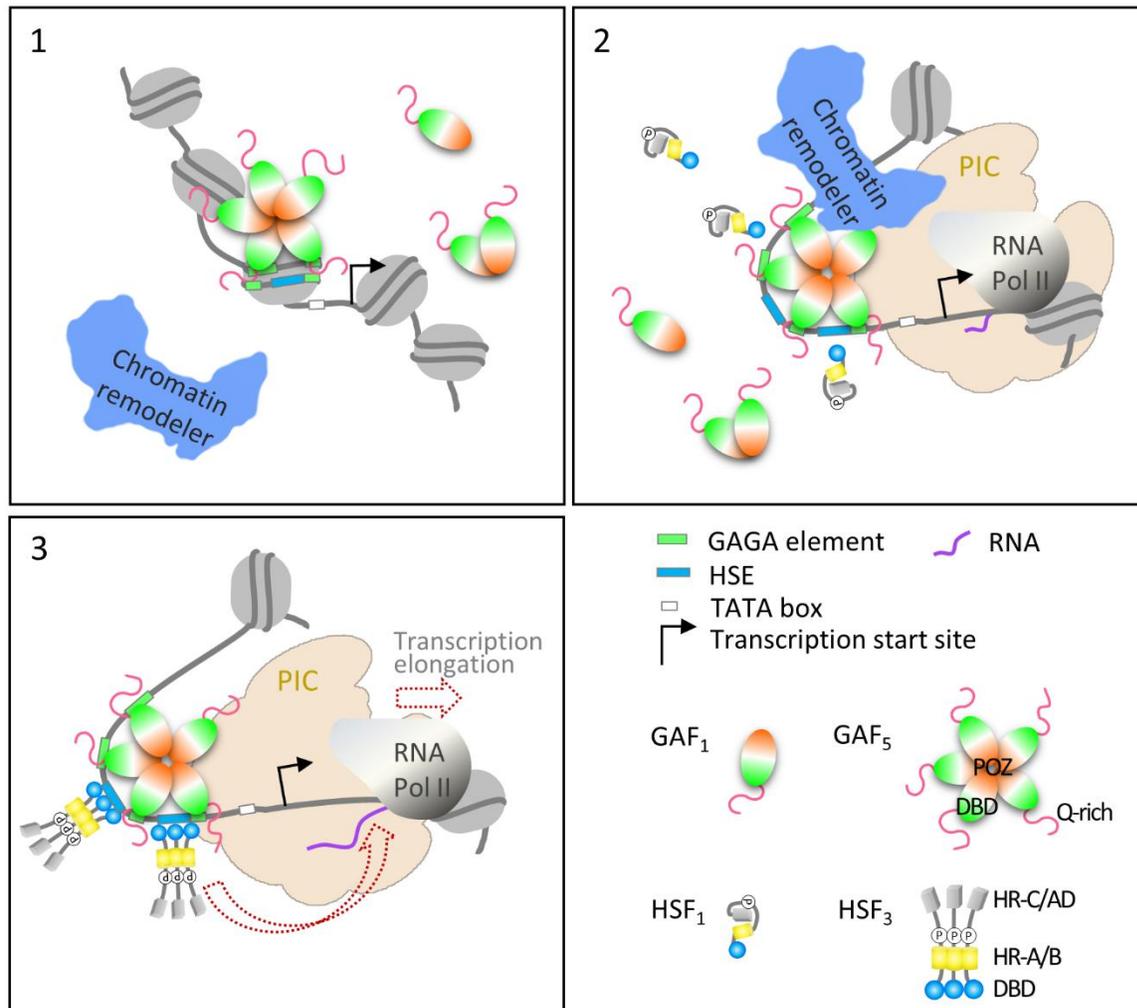


Figure 6. Pioneering of chromatin accessibility is a process involving multiple inputs

Model: GAF binds autonomously to nucleosomal sites at the first stage of pioneering (box 1). High GAF occupancy at a *Hsp* promoter with clustered GAGA elements maintains chromatin accessibility for neighboring factor HSF and assembly of the preinitiation complex and paused RNA Pol II (box 2). The substantially constrained diffusivity (D_{bound}) of stably bound GAF may reflect multisite interactions of a GAF multimer with clustered GAGA elements (Katsani et al, 1999), locking down GAF with prolonged residence time. HSF trimers bind to accessible chromatin DNA with high affinity on heat shock to trigger RNA Pol II elongation (box 3). See discussion for details.

Methods

Fly strain construction

CRISPR/Cas9-mediated genome editing

HaloTag was inserted downstream of the start codon of endogenous *Trl* via homology-directed repair (HDR) and CRISPR/Cas9 to generate the Halo-GAF knock-in strain (**Fig. S1 A-C**). The donor repair template was constructed on the pScarlessHD-DsRed plasmid (a gift from Kate O'Connor-Giles, Addgene plasmid # 64703), which contains a DsRed selection marker cassette flanked by PBac transposon ends and TTAA sites⁹⁷. The donor plasmid was designed such that after HDR, the DsRed cassette is inserted into a nearby genomic TTAA site adjacent to the gRNA target in the coding region that is close to the ATG start codon. Approximately 1 kb downstream of the gRNA site was cloned as the right homology arm (RHA), with silent mutations introduced to destroy the gRNA sequence in the donor plasmid. Similarly, 1kb upstream of the genomic TTAA site was cloned as the left homology arm (LHA). LHA and RHA mediate HDR upon Cas9 cleavage, inserting HaloTag along with the DsRed cassette. Flies that underwent HDR were identified with DsRed eye fluorescence. The DsRed cassette was removed with a single cross to a fly strain expressing PBac transposase, as indicated by loss of fluorescence, leaving only one TTAA site, thus allowing scarless HaloTag knock-in with a removable selection marker. A flexible linker GGSGS was added between Halo and GAF. The HaloTag knock-in was verified by fluorescent staining and DNA sequencing.

After constructing the Halo-GAF strain, deletions of the Halo-GAF fusion protein were generated by CRISPR-Cas9 gene editing. A 90 bp (30 AA, Δ 90-119) precise deletion was generated in the POZ domain (Δ POZ) by HDR. Small deletions in the zinc finger of the DBD (ZF^9 , R356 Δ , N357 Δ ; and ZF^{10} , R356 Δ) were generated by random indels. For Δ Q, two gRNAs targeting the Q-rich domains of the long or short GAF isoforms were introduced at the same time to screen for indels creating frameshifts and truncations of both Q-rich domains. To screen for desired mutants, lethal or reduced viability strains were selected and characterized by PCR and DNA sequencing.

All gRNAs were cloned into pCFD5. Donor and gRNA plasmids were mixed to a final concentration of 200ng/uL and 500~600ng/uL, respectively, and injected into fly strains expressing Cas9 in the germline (*yw;nos-Cas9(II-attP40)*, a gift from NIG-FLY, Japan). To generate Halo-GAF mutants, the Halo-GAF knock-in strain was crossed to *yw;nos-Cas9(II-attP40)* for injection. All fly embryo injections were performed by BestGene Inc (CA).

Transgenic fly construction via PhiC31 integrase

Trl gene and ~1kb flanking genomic sequence was cloned from a BAC genomic clone (BACR11B23) into *pattB* (backbone taken from *pattB-aubergine-ADH-gf*, Addgene plasmid # 69448, a gift from Phillip Zamore) via recombineering⁹⁸. HaloTag was inserted upstream of the

stop codon for the long and short isoforms, respectively, along with a removable Cam^R selection cassette via recombineering⁹⁹. The Cam^R cassette was flanked by the 8-bp NotI restriction sites (plus an additional bp to ensure that Halotag is in frame) and removed by NotI digestion and re-ligation, leaving a GGSGSAAA linker sequence between GAF and Halotag. The constructs were incorporated into the attP2 site in the *Drosophila* genome via PhiC31 integrase¹⁰⁰ (**Fig. S1E**), generating the GAF^L-Halo and GAF^S-Halo transgenic strains, which express a HaloTagged long or short GAF isoform and the other untagged isoform. The functionality of recombinant fusion proteins was verified by rescue of the lethal alleles *Trl^{13C}/Trl^{R67}*³. We similarly generated the HSF-Halo transgenic fly strain at the attP2 site from the genomic clone BACR33K09. The functionality of HSF-Halo was verified by rescue of *P{PZ}Hsf⁰³⁰⁹¹/Hsf³* lethal alleles^{58,59}. The Halo-H2B transgenic strain was similarly constructed at the attP2 site, with a ~4.9 kb DNA fragment containing five *Drosophila* histone genes for Halotag insertion at the N-terminus of H2B.

Mutant fly strains

Mutant alleles were obtained from the Bloomington *Drosophila* Stock center (BDSD, IN): *Trl^{13C}* (BDSC:58473); *Trl^{R67}* (BDSC:58475); *P{PZ}Hsf⁰³⁰⁹¹* (BDSC:11271); *Hsf³* (BDSC:5488); *P{EP}Bap170^{G5986}* (BDSC:28471); *Bap170^{Δ135}* (BDSC:63807); *Nurf301⁴* (BDSC:9904); and *Df(3L)Exel6084* (BDSC:7563).

Genotypes of fly strains in Fig. 3 and Fig. S6 (only GAF^L-Halo isoform is shown, GAF^S-Halo strains have the same corresponding genotypes except expressing GAF^S-Halo):

WT: p{GAF^L-Halo}attP2

bap170: Bap170^{Δ135}/P{EP}Bap170^{G5986}; p{GAF^L-Halo}attP2 (generated by crossing *Bap170^{Δ135}; p{GAF^L-Halo}attP2/T(2;3)TSTL, CyO: TM6B, Tb¹* to *P{EP}Bap170^{G5986}; p{GAF^L-Halo}attP2/ T(2;3)TSTL, CyO: TM6B, Tb¹*)

nurf301: Nurf301⁴, p{GAF^L-Halo}attP2/Df(3L)Exel6084, p{GAF^L-Halo}attP2 (generated by crossing *Nurf301⁴, p{GAF^L-Halo}attP2/TM6B, Tb¹* to *Df(3L)Exel6084, p{GAF^L-Halo}attP2/TM6B, Tb¹*)

Genotypes of fly strains in Fig. S8A:

WT: p{HSF-Halo}attP2

trl: Trl^{13C}, p{HSF-Halo}attP2/Trl^{R67}, p{HSF-Halo}attP2 (generated by crossing *Trl^{13C}, p{HSF-Halo}attP2/TM6B, Tb¹* to *Trl^{R67}, p{HSF-Halo}attP2/TM6B, Tb¹*)

bap170: Bap170^{Δ135}/P{EP}Bap170^{G5986}; p{HSF-Halo}attP2 (generated by crossing *Bap170^{Δ135}; p{HSF-Halo}attP2/T(2;3)TSTL, CyO: TM6B, Tb¹* to *P{EP}Bap170^{G5986}; p{HSF-Halo}attP2/ T(2;3)TSTL, CyO: TM6B, Tb¹*)

nurf301: *Nurf301*⁴, *p{HSF-Halo}attP2/Df(3L)Exel6084*, *p{HSF-Halo}attP2* (generated by crossing *Nurf301*⁴, *p{HSF-Halo}attP2/TM6B*, *Tb*¹ to *Df(3L)Exel6084*, *p{HSF-Halo}attP2/TM6B*, *Tb*¹)

Single-particle imaging in live *Drosophila* hemocytes

Sample preparation

Single-molecule live cell imaging was performed with 3rd instar larval hemocytes, representing mainly plasmatocytes (>90% of *Drosophila* hemocytes). Hemocytes were released from 5-10 thoroughly washed larvae into a sample chamber containing 1 mL filtered Schneider's *Drosophila* medium (Gibco™ 21720024) including an EDTA-free protease inhibitor cocktail (Roche 4693159001). The sample chamber is an Attofluor™ Cell Chamber (Invitrogen, A7816) assembled with round coverglass (Electron Microscopy Sciences, 72290-12) cleaned by flaming. Cells were stained with 0.2~1.5 nM JF552/JFX554 for 30 min at room temperature, during which hemocytes adhered to the coverglass bottom of the imaging chamber. During incubation steps, sample chambers were covered with aluminum foil to minimize evaporation and block light. Cells were then briefly washed twice with Schneider's media without protease inhibitor and imaged on a custom-built wide-field SPT fluorescence microscope¹⁰¹.

Single-particle imaging

All single-particle imaging were carried out on an Axio Observer Z1 microscope (Zeiss, Germany) equipped with an Plan-Apochromat 150x/1.35 glycerin-immersion objective (ZEISS, Germany), and a C9100-13 EM-CCD camera (Hamamatsu Photonics, Japan) featuring 512x512 pixels with 16 μm pixel size. The pixel size of recorded images is 16 μm/150 = 107 nm. JF552/JFX554 were excited with a CL555-100 555 nm laser (CrystaLaser, Reno, NV) and the emission light was passed through a filter cube containing a 561 nm BrightLine single-edge beamsplitter, a 612/69 nm BrightLine single-band bandpass emission filter (Semrock, Rochester, NY), then through a 750 nm blocking edge BrightLine multiphoton short-pass emission filter and a 405/488/561/635 nm StopLine quad-notch filter (Semrock, Rochester, NY) before entering the camera. The EM-CCD camera was operated at ~-80°C (forced-air cooling) and 1200x EM gain. We used the ZEN (ZEISS, Germany) and HClmage (Hamamatsu Photonics, Japan) software to operate the microscope and camera, respectively. Imaging was carried out at room temperature except for heat shock experiments in which samples were imaged in a stage-top incubator with temperature control (H301-MINI chamber with UNO-T-H controller, Okolab, Italy)

In the fast-tracking regime, time-lapse movies with a 128x128 pixel field of view were acquired with high laser power (~1 kW/cm²) and 10 ms exposure time for 1.5-2 min. Initial laser excitation leads to simultaneous emissions of all labeled molecules, marking locations of individual nuclei in the field of view. Cells with relatively homogenous initial nuclear glow (interphase) were imaged. Emitting molecules quickly enter the "dark" state and stochastically reemit. Cells were stained with JFX554, with the concentration optimized (1-1.5 nM) to achieve

sparse single-particles per nucleus per frame after 10~30 s of the initial glow, minimizing mis-tracking.

For slow tracking, we used low laser power ($\sim 36 \text{ W/cm}^2$) and imaged a 256x256 pixel field of view with 500 ms exposure time for 2-5 min. We labeled cells with 50 nM of a far-red dye JF700 to block most Halo-tagged proteins and at the same time adjusted a low concentration of JF552 to visualize only 2-10 molecules/frame. This sparse labeling approach allows tracking of chromatin-bound molecules with minimal photobleaching.

Single-particle data processing and statistical analysis

Image pre-processing

Raw time-lapse data were pre-processed in Fiji¹⁰² to convert to 16-bit TIFF format and extract a substack with sparse single particles (<5 particles/nucleus for fast tracking, and < 10 particles/nucleus for slow tracking). A maximum-intensity Z projection of each movie was generated to outline cell nuclei as the ROI. A corresponding binary mask was created to isolate nuclear trajectories for subsequent analysis.

Single-particle localizing and tracking

Single particles were localized and tracked using the open-source program DiaTrack v3.05¹⁰³. Tracking was performed with a 6 pixel ($\sim 0.65 \mu\text{m}$) maximum jump allowance between consecutive frames for fast tracking. All factors we imaged showed displacements within this cut-off as informed by the frequency histogram (**Fig. S2B, S5A, S6A, and S7B**). Since slow tracking selectively imaged bound particles, the maximum jump allowance between consecutive frames was set as 3 pixels ($\sim 0.32 \mu\text{m}$) to minimize misconnection. HSF-Halo showed displacement histograms with a smooth tail within this range, while Halo-GAF and Halo-H2B displacements were mostly within $0.2 \mu\text{m}$ (not shown). For analysis of slow-tracking experiments to measure residence times, we allowed gaps in trajectories to account for blinking or missed localizations, with 3-frame maximum blinking and a more stringent 2-pixel maximum jump.

Analyzing fast-tracking data

We used a custom R package Sojourner (<https://github.com/sheng-liu/sojourner>) to extract trajectories from MATLAB files generated by DiaTrack, which contain information on x, y coordinates and frame number (time) that were applied for computation of kinetic parameters. Trajectories found within the nucleus were isolated ('masked' trajectories) using Sojourner and binary masks generated during pre-processing. Average length of trajectories was 11-21 displacements (median = 5-8).

Spot-On

We used Spot-on to perform two-state kinetic modeling of displacements from all 'masked' trajectories³³, to derive diffusion coefficients (D_{bound} , D_{free}) and the corresponding fractions

(F_{bound} , $F_{\text{free}}=1-F_{\text{bound}}$). The Spot-On python package was used with the following parameters: bin width = 0.01 μm , number of timepoints = 6, jumps to consider = 4, max jump = 1 μm , gapsAllowed = 0, and Z correction with $dZ = 0.6 \mu\text{m}$. Mean and SD of F_{bound} , D_{bound} and D_{free} were calculated from 3-5 biological replicates.

vbSPT (variational Bayesian single-particle tracking) HMM

A matlab program running vbSPT HMM^{63,64} (<https://gitlab.com/anders.sejr.hansen/anisotropy>) was modified to assign each trajectory displacement into two states, 'bound' or 'free'. Then each trajectory was sub-classified as 'bound' if all displacements are classified as bound state; 'free' if all displacements are classified as free state; a small fraction of trajectories containing two states were omitted from related analysis. The sub-classified 'bound' and 'free' trajectories from biological replicates of the same conditions were pooled together and used to calculate mean squared displacements (MSD).

To calculate the apparent radius of confinement (R_c) for individual trajectories, we fit each MSD curve with the following confined diffusion model^{36,104},

$$MSD = R_c \times \left(1 - e^{-\frac{4D\Delta t}{R_c^2}}\right)$$

Analyzing slow-tracking data

Using the Sojourner R package, the apparent dwell times (temporal length of trajectories) were determined for all "masked" trajectories lasting at least 3 frames.

1-CDF curves were generated and fit to a double exponential decay model:

$$P(t) = f_{sb}e^{-k_{sb}t} + f_{tb}e^{-k_{tb}t}$$

where k_{sb} and k_{tb} correspond to dissociation rates for stable- and transient-binding events, respectively; f_{sb} and f_{tb} correspond to the fraction of time the molecule spends at stable- and transient-binding sites, respectively, and $f_{sb} + f_{tb} = 1$.

The survival curves reflect not only factor dissociation, but also photobleaching, axial and lateral cell or chromatin movements, fluctuating background, etc. To correct for all these factors, assuming that these processes affect Halo-H2B to the same extent as other proteins, and that bulk H2B dissociation is negligible in the experimental time frame of 2-5 min, we measured the apparent unbinding rate for Halo-H2B in the same way and used it as a correction factor for other proteins' residence time³⁸. The corrected average residence times for stable- (τ_{sb}) and transient-binding (τ_{tb}) were calculated as follows:

$$\tau_{sb} = \frac{1}{k_{sb} - k_{sb,H2B}}$$

$$\tau_{tb} = \frac{1}{k_{tb} - k_{sb,H2B}}$$

Mean and SD of k_{sb} , k_{tb} , f_{sb} and f_{tb} were calculated from 100 bootstrap samples, then mean and SD of k_{sb} and k_{tb} were used to calculate τ_{sb} and τ_{tb} with error propagation.

Calculating search kinetics and target occupancy

We integrated approaches from previous studies^{32,105,106} and calculated temporal occupancy as described⁷².

First, search time (τ_{search}) is the average time it takes from a molecule dissociates off a specific site till it find the next specific site, during which the molecule samples nonspecific sites (each lasts for τ_{tb} on average) for a number of times (N_{trials}) before encountering the next specific target (bound for τ_{sb} on average). τ_{free} is the average free time between two non-specific binding events. Assuming the molecule samples all non-specific and specific sites at random with equal accessibility, i.e. equal probability of binding to all sites, the average search time between two consecutive specific binding events is calculated as:

$$\tau_{search} = N_{trials} \times (N_{trials} + 1) \times \tau_{free}$$

N_{trials} depends on the ratio of number of non-specific (N_{ns}) to specific sites (N_s), or r_s :

$$N_{trials} = \frac{N_s + N_{ns}}{N_s} = 1 + r_s$$

Thus,

$$\tau_{search} = (1 + r_s) \times \tau_{tb} + (2 + r_s) \times \tau_{free}$$

To determine r_s , we considered two scenarios underlying detection of binding events during slow tracking⁷².

- (a) Blinking-limited ($r_{s,bl.}$): f_{sb} obtained by slow tracking is proportional to the fraction of time the molecule spends at specific sites (stable-binding) relative to the overall time it is bound to chromatin (stable- and transient-binding):

$$f_{sb} = \frac{N_s \times \tau_{sb}}{N_s \times \tau_{sb} + N_{ns} \times \tau_{tb}} = \frac{\tau_{sb}}{\tau_{sb} + r_s \times \tau_{tb}}$$

$$r_{s,bl.} = \frac{\tau_{sb}}{\tau_{tb}} \times \left(\frac{1}{f_{sb}} - 1 \right)$$

- (b) Diffusion-limited ($r_{s,diff.}$): assuming equal probability of binding to all sites, f_{sb} depends on the ratio of number of specific sites to all sites:

$$f_{sb} = \frac{N_s}{N_s + N_{ns}} = \frac{1}{1 + r_s}$$

$$r_{s,diff.} = \frac{1}{f_{sb}} - 1$$

These physical processes can happen in the cell coincidentally and likely represent two extremes of a spectrum of behaviors single molecules can exhibit. We reasoned that the relative likelihood of detecting a blinking-limited binding event by slow tracking is proportional to the global fraction of bound molecules (F_{bound} obtained by fast tracking). Therefore, we computed a weighted average value for r_s as follows:

$$r_s = \frac{(F_{bound} \times r_{s,bl.}) + (1 - F_{bound}) \times r_{s,diff.}}{2}$$

To obtain τ_{free} , we considered that F_{bound} is proportional to the fraction of the time a molecule spends bound to chromatin either stably or transiently:

$$F_{bound} = \frac{\tau_{sb} + N_{trials} \times \tau_{tb}}{\tau_{sb} + N_{trials} \times \tau_{tb} + (N_{trials} + 1) \times \tau_{free}}$$

Thus,

$$\tau_{free} = \frac{\frac{(1 + r_s) \times \tau_{tb} + \tau_{sb}}{F_{bound}} - (1 + r_s) \times \tau_{tb} - \tau_{sb}}{2 + r_s}}$$

τ_{search} was calculated with the values derived for r_s and τ_{free} , as shown above. We then estimated the sampling interval (SI), the average time between two consecutive binding events at a specific site ³²,

$$SI = \frac{(\tau_{search} + \tau_{sb}) \times N_{sites}}{N \text{ molecules}}$$

We used N_{sites} values presented by GAF and HSF ChIP-seq studies^{17,48}. $N_{molecules}$ was estimated by flow cytometry (see below). Finally, the average occupancy is the percentage of time a given specific site is occupied by the protein of interest:

$$Occupancy = \frac{\tau_{sb}}{SI}$$

Confocal microscopy

Hemocytes were prepared in the same way described above for live-cell imaging, except for staining with 50 nM JFX554 for 30 min at room temperature or heat shocked on a metal heat block at the indicated temperature (the time for heat shock overlaps with the final stage of staining so that dye labeling and heat shock were completed at the same time). During all incubation steps the sample chambers were covered with aluminum foil to minimize evaporation and block light. Then cells were briefly washed twice with PBS and immediately fixed in freshly made 4% formaldehyde (diluted from Pierce™ 16% Formaldehyde (w/v), Methanol-free, #28906) in 1X PBS for 15 min. Fixed samples were washed in PBS for 10 min, then stained with DAPI for 10 min and washed in PBS for 5 min. Sample chambers were filled with PBS and covered by a coverglass on top. Salivary glands were dissected, then stained and

heat-shocked similarly as hemocytes except that JF554 staining was performed after fixation. Salivary gland samples were mounted on glass slides in VECTASHIELD® Antifade Mounting Medium (Vector Labs H-1000-10). We imaged these samples on a LSM800 Airyscan confocal microscope (Zeiss, Germany) with a 63X objective. Z-stacks were taken with 0.2 μm step size for hemocyte nuclei and 0.5 μm step size for salivary gland polytene nuclei. The same laser and scanning settings were used between samples in the same experiment.

Estimation of cellular abundances for Halo-tagged proteins by flow cytometry

Cellular abundances of Halo-GAF and HSF-Halo were estimated by flow cytometry using a calibrated C32 CTCF-Halo U2OS human cell line^{81,107}. U2OS cell samples were prepared as described¹⁰⁷ with minor modifications. Briefly, we labeled WT and CTCF-Halo U2OS cells with 50 nM JF552 for 30 min at 37°C/5% CO₂ in a tissue-culture incubator, washed out the dye (removed medium; rinsed with PBS, and incubated with fresh media for 5 min in the incubator) and then immediately prepared cells for flow cytometry. Resuspended cells were filtered through a 40 μm filter and placed on ice until their fluorescence was read out by the flow cytometer. To prepare fly hemocytes for flow cytometry, 20~30 3rd instar larvae were thoroughly washed and dissected on ice in a 1.5 mL eppendorf tube lid containing Schneider's *Drosophila* medium (Gibco™ 21720024), EDTA-free protease inhibitor cocktail (Roche 4693159001) and 10% FBS (HyClone FBS SH30910.03, Cytiva, MA). Hemocytes were collected and stored on ice. After dissection was done for all fly strains, hemocytes were stained with 50nM JF552 in 1mL medium at room temperature for 30 min. All tubes were pre-rinsed with FBS to minimize cell stickiness to the tubes. After staining, hemocytes were centrifuged at 200 x g for 5 min, resuspended in 1 mL fresh medium and washed at room temperature for 15 min (longer wash time than for U2OS cells to remove non-specific cytoplasmic signals). The hemocytes were centrifuged again, resuspended in 500 μL medium and placed on ice until their fluorescence was read out by the flow cytometer.

We used a SH800 (Sony, Japan) cell sorter in analyze mode to measure fluorescence intensity in the U2OS cell lines and hemocytes with the same settings. Single live cells were gated using forward and side scattering. JF552 fluorescence was excited using a 561 nm laser and emission read out using a 617/30 band pass filter. The absolute abundance of protein of interest $N_{molecules}$ (mean number of molecules per cell) was obtained according to:

$$N_{molecules} = \frac{I - I_{Background}}{I_{CTCF} - I_{U2OSBackground}} \times N_{CTCF}$$

Where I is the average measured fluorescence intensity of the cells expressing the protein of interest, $I_{Background}$ is the average measured fluorescence intensity of hemocytes from a fly strain not expressing Halotag (*w1118*), I_{CTCF} is the average measured fluorescence intensity of the CTCF-Halo standard U2OS cell line, $I_{U2OSBackground}$ is the average measured fluorescence intensity of WT U2OS cells not expressing Halotag, and N_{CTCF} is the absolute abundance of CTCF-Halo (~109,800 proteins per cell). For each experiment, hemocytes and U2OS cells were stained with

the same aliquot of JF552 stock solution and measured during the same flow cytometry session. We performed three to five biological replicates to get mean and standard deviation values.

Characterization of cell cycle stage for larval hemocytes using the Fly-Fucci system

A fly strain with the Fly-Fucci markers under UAS control (UAS-CFP.E2f1.1-230 and UAS-Venus.NLS.CycB.1-266, BDSC:55122) was crossed to a hemocyte-specific driver Cg-Gal4 (BDSC:7011). 3rd instar larvae were washed then dissected to release hemocytes in a drop of PBS on a slide, then the fluorescence of hemocytes were imaged immediately on a Zeiss Axioplan 2 compound microscope.

ACKNOWLEDGEMENTS

We thank Anders Hansen and Maxime Woringer for discussion on Spot-On analyses, Anders Hansen, Claudia Cattoglio, Xavier Darzacq and Robert Tjian for the CTCF-Halo U2OS cell line and discussions on measuring factor abundance, Tim Lionnet, James Zhe Liu, Peng Dong, and Brian Mehl for advice on SPT, Yick Hin Ling and Sun Jay Yoo for assistance with data analysis, Pascal Vallotton for customization of DiaTrack software, Paul Badenhorst for advice on larval hemocyte culture, Steve Deluca for advice on bioinformatics, Weina Dai for imaging assistance, Erin Pryce and the Integrated Imaging Center for LSM 800 training, Yundong Liu for assembly and maintenance of a high performance computational platform, John Lis, Mike Levine, and Gordon Hager for discussion, and Wu Lab members for comments on the manuscript. This study was supported by HHMI funding to the TIC (C.W., Q.Z., and L.L.), Johns Hopkins Bloomberg Distinguished Professorship funds (C.W.), and National Institutes of Health grants GM132290-01 (C.W.) and DK127432 (C.W.).

AUTHOR CONTRIBUTIONS

X.T. performed all genetic and imaging experiments with support from T.L., J.W., and Y.R. and all data analysis using R functions created by S.L. and X.T.. L.D.L. and Q.Z. synthesized JF552/JFX554 and JF700. X.T. and C.W. designed the study and wrote the paper with input from all authors.

REFERENCES

1. Biggin, M. D. & Tjian, R. Transcription factors that activate the Ultrabithorax promoter in developmentally staged extracts. *Cell* **53**, 699–711 (1988).
2. Gilmour, D. S., Thomas, G. H. & Elgin, S. C. Drosophila nuclear proteins bind to regions of

- alternating C and T residues in gene promoters. *Science* **245**, 1487–1490 (1989).
3. Farkas, G. *et al.* The Trithorax-like gene encodes the Drosophila GAGA factor. *Nature* **371**, 806–808 (1994).
 4. Soeller, W. C., Oh, C. E. & Kornberg, T. B. Isolation of cDNAs encoding the Drosophila GAGA transcription factor. *Mol. Cell. Biol.* **13**, 7961–7970 (1993).
 5. Chopra, V. S. *et al.* Transcriptional activation by GAGA factor is through its direct interaction with dmTAF3. *Dev. Biol.* **317**, 660–670 (2008).
 6. Lomaev, D. *et al.* The GAGA factor regulatory network: Identification of GAGA factor associated proteins. *PLoS One* **12**, e0173602 (2017).
 7. Giot, L. *et al.* A protein interaction map of Drosophila melanogaster. *Science* **302**, 1727–1736 (2003).
 8. Li, J. *et al.* Kinetic competition between elongation rate and binding of NELF controls promoter-proximal pausing. *Mol. Cell* **50**, 711–722 (2013).
 9. Croston, G. E., Kerrigan, L. A., Lira, L. M., Marshak, D. R. & Kadonaga, J. T. Sequence-specific antirepression of histone H1-mediated inhibition of basal RNA polymerase II transcription. *Science* **251**, 643–649 (1991).
 10. Cirillo, L. A. & Zaret, K. S. An early developmental transcription factor complex that is more stable on nucleosome core particles than on free DNA. *Mol. Cell* **4**, 961–969 (1999).
 11. Soufi, A. *et al.* Pioneer transcription factors target partial DNA motifs on nucleosomes to initiate reprogramming. *Cell* **161**, 555–568 (2015).
 12. Tsukiyama, T., Becker, P. B. & Wu, C. ATP-dependent nucleosome disruption at a heat-shock promoter mediated by binding of GAGA transcription factor. *Nature* **367**, 525–532

- (1994).
13. Okada, M. & Hirose, S. Chromatin remodeling mediated by Drosophila GAGA factor and ISWI activates fushi tarazu gene transcription in vitro. *Mol. Cell. Biol.* **18**, 2455–2461 (1998).
 14. Nakayama, T., Shimojima, T. & Hirose, S. The PBAP remodeling complex is required for histone H3.3 replacement at chromatin boundaries and for boundary functions. *Development* **139**, 4582–4590 (2012).
 15. Xiao, H. *et al.* Dual functions of largest NURF subunit NURF301 in nucleosome sliding and transcription factor interactions. *Mol. Cell* **8**, 531–543 (2001).
 16. Sherwood, R. I. *et al.* Discovery of directional and nondirectional pioneer transcription factors by modeling DNase profile magnitude and shape. *Nat. Biotechnol.* **32**, 171–178 (2014).
 17. Fuda, N. J. *et al.* GAGA factor maintains nucleosome-free regions and has a role in RNA polymerase II recruitment to promoters. *PLoS Genet.* **11**, e1005108 (2015).
 18. Duarte, F. M. *et al.* Transcription factors GAF and HSF act at distinct regulatory steps to modulate stress-induced gene activation. *Genes Dev.* **30**, 1731–1746 (2016).
 19. Badenhorst, P., Voas, M., Rebay, I. & Wu, C. Biological functions of the ISWI chromatin remodeling complex NURF. *Genes Dev.* **16**, 3186–3198 (2002).
 20. Boija, A. *et al.* CBP Regulates Recruitment and Release of Promoter-Proximal RNA Polymerase II. *Mol. Cell* **68**, 491–503.e5 (2017).
 21. Kuroda, M. I., Kang, H., De, S. & Kassis, J. A. Dynamic Competition of Polycomb and Trithorax in Transcriptional Programming. *Annu. Rev. Biochem.* **89**, 235–253 (2020).

22. Wolle, D. *et al.* Functional Requirements for Fab-7 Boundary Activity in the Bithorax Complex. *Mol. Cell. Biol.* **35**, 3739–3752 (2015).
23. van Steensel, B., Delrow, J. & Bussemaker, H. J. Genomewide analysis of Drosophila GAGA factor target genes reveals context-dependent DNA binding. *Proc. Natl. Acad. Sci. U. S. A.* **100**, 2580–2585 (2003).
24. Judd, J., Duarte, F. M. & Lis, J. T. Pioneer-like factor GAF cooperates with PBAP (SWI/SNF) and NURF (ISWI) to regulate transcription. *Genes Dev.* **35**, 147–156 (2021).
25. Gaskill, M. M., Gibson, T. J., Larson, E. D. & Harrison, M. M. GAF is essential for zygotic genome activation and chromatin accessibility in the early embryo. *Elife* **10**, (2021).
26. Benyajati, C. *et al.* Multiple isoforms of GAGA factor, a critical component of chromatin structure. *Nucleic Acids Res.* **25**, 3345–3353 (1997).
27. Greenberg, A. J. & Schedl, P. GAGA factor isoforms have distinct but overlapping functions in vivo. *Mol. Cell. Biol.* **21**, 8565–8574 (2001).
28. Tepass, U., Fessler, L. I., Aziz, A. & Hartenstein, V. Embryonic origin of hemocytes and their relationship to cell death in Drosophila. *Development* **120**, 1829–1837 (1994).
29. Read, D., Butte, M. J., Dernburg, A. F., Frasch, M. & Kornberg, T. B. Functional studies of the BTB domain in the Drosophila GAGA and Mod(mdg4) proteins. *Nucleic Acids Res.* **28**, 3864–3870 (2000).
30. Rust, M. J., Bates, M. & Zhuang, X. Sub-diffraction-limit imaging by stochastic optical reconstruction microscopy (STORM). *Nat. Methods* **3**, 793–795 (2006).
31. Heilemann, M. *et al.* Subdiffraction-resolution fluorescence imaging with conventional fluorescent probes. *Angew. Chem. Int. Ed Engl.* **47**, 6172–6176 (2008).

32. Chen, J. *et al.* Single-molecule dynamics of enhanceosome assembly in embryonic stem cells. *Cell* **156**, 1274–1285 (2014).
33. Hansen, A. S. *et al.* Robust model-based analysis of single-particle tracking experiments with Spot-On. *Elife* **7**, (2018).
34. Chong, S. *et al.* Imaging dynamic and selective low-complexity domain interactions that control gene transcription. *Science* **361**, (2018).
35. Swinstead, E. E. *et al.* Steroid Receptors Reprogram FoxA1 Occupancy through Dynamic Chromatin Transitions. *Cell* **165**, 593–605 (2016).
36. Lerner, J. *et al.* Two-Parameter Mobility Assessments Discriminate Diverse Regulatory Factor Behaviors in Chromatin. *Mol. Cell* **79**, 677–688.e6 (2020).
37. Liu, H. *et al.* Visualizing long-term single-molecule dynamics in vivo by stochastic protein labeling. *Proc. Natl. Acad. Sci. U. S. A.* **115**, 343–348 (2018).
38. Hansen, A. S., Pustova, I., Cattoglio, C., Tjian, R. & Darzacq, X. CTCF and cohesin regulate chromatin loop stability with distinct dynamics. *Elife* **6**, (2017).
39. Espinás, M. L. *et al.* The N-terminal POZ domain of GAGA mediates the formation of oligomers that bind DNA with high affinity and specificity. *J. Biol. Chem.* **274**, 16461–16469 (1999).
40. Katsani, K. R., Hajibagheri, M. A. & Verrijzer, C. P. Co-operative DNA binding by GAGA transcription factor requires the conserved BTB/POZ domain and reorganizes promoter topology. *EMBO J.* **18**, 698–708 (1999).
41. Wilkins, R. C. & Lis, J. T. DNA distortion and multimerization: novel functions of the glutamine-rich domain of GAGA factor. *J. Mol. Biol.* **285**, 515–525 (1999).

42. Tsukiyama, T. & Wu, C. Purification and properties of an ATP-dependent nucleosome remodeling factor. *Cell* **83**, 1011–1020 (1995).
43. Badenhorst, P. *et al.* The *Drosophila* nucleosome remodeling factor NURF is required for Ecdysteroid signaling and metamorphosis. *Genes Dev.* **19**, 2540–2545 (2005).
44. Chalkley, G. E. *et al.* The transcriptional coactivator SAYP is a trithorax group signature subunit of the PBAP chromatin remodeling complex. *Mol. Cell. Biol.* **28**, 2920–2929 (2008).
45. Yen, K., Vinayachandran, V., Batta, K., Koerber, R. T. & Pugh, B. F. Genome-wide nucleosome specificity and directionality of chromatin remodelers. *Cell* **149**, 1461–1473 (2012).
46. Shopland, L. S., Hirayoshi, K., Fernandes, M. & Lis, J. T. HSF access to heat shock elements in vivo depends critically on promoter architecture defined by GAGA factor, TFIID, and RNA polymerase II binding sites. *Genes Dev.* **9**, 2756–2769 (1995).
47. Lis, J. T., Mason, P., Peng, J., Price, D. H. & Werner, J. P-TEFb kinase recruitment and function at heat shock loci. *Genes Dev.* **14**, 792–803 (2000).
48. Guertin, M. J. & Lis, J. T. Chromatin landscape dictates HSF binding to target DNA elements. *PLoS Genet.* **6**, e1001114 (2010).
49. Lis, J. & Wu, C. Protein traffic on the heat shock promoter: parking, stalling, and trucking along. *Cell* **74**, 1–4 (1993).
50. Vuister, G. W. *et al.* Solution structure of the DNA-binding domain of *Drosophila* heat shock transcription factor. *Nat. Struct. Biol.* **1**, 605–614 (1994).
51. Kim, S. J., Tsukiyama, T., Lewis, M. S. & Wu, C. Interaction of the DNA-binding domain of *Drosophila* heat shock factor with its cognate DNA site: a thermodynamic analysis using

- analytical ultracentrifugation. *Protein Sci.* **3**, 1040–1051 (1994).
52. Westwood, J. T., Clos, J. & Wu, C. Stress-induced oligomerization and chromosomal relocation of heat-shock factor. *Nature* **353**, 822–827 (1991).
53. Baler, R., Dahl, G. & Voellmy, R. Activation of human heat shock genes is accompanied by oligomerization, modification, and rapid translocation of heat shock transcription factor HSF1. *Mol. Cell. Biol.* **13**, 2486–2496 (1993).
54. Sarge, K. D., Murphy, S. P. & Morimoto, R. I. Activation of heat shock gene transcription by heat shock factor 1 involves oligomerization, acquisition of DNA-binding activity, and nuclear localization and can occur in the absence of stress. *Mol. Cell. Biol.* **13**, 1392–1407 (1993).
55. Perisic, O., Xiao, H. & Lis, J. T. Stable binding of Drosophila heat shock factor to head-to-head and tail-to-tail repeats of a conserved 5 bp recognition unit. *Cell* **59**, 797–806 (1989).
56. Neudegger, T., Verghese, J., Hayer-Hartl, M., Hartl, F. U. & Bracher, A. Structure of human heat-shock transcription factor 1 in complex with DNA. *Nat. Struct. Mol. Biol.* **23**, 140–146 (2016).
57. Westwood, J. T. & Wu, C. Activation of Drosophila heat shock factor: conformational change associated with a monomer-to-trimer transition. *Mol. Cell. Biol.* **13**, 3481–3486 (1993).
58. Spradling, A. C. *et al.* The Berkeley Drosophila Genome Project gene disruption project: Single P-element insertions mutating 25% of vital Drosophila genes. *Genetics* **153**, 135–177 (1999).
59. Jedlicka, P., Mortin, M. A. & Wu, C. Multiple functions of Drosophila heat shock

- transcription factor in vivo. *EMBO J.* **16**, 2452–2462 (1997).
60. Yao, J., Munson, K. M., Webb, W. W. & Lis, J. T. Dynamics of heat shock factor association with native gene loci in living cells. *Nature* **442**, 1050–1053 (2006).
 61. Chowdhary, S., Kainth, A. S., Pincus, D. & Gross, D. S. Heat Shock Factor 1 Drives Intergenic Association of Its Target Gene Loci upon Heat Shock. *Cell Rep.* **26**, 18–28.e5 (2019).
 62. Gaglia, G. *et al.* HSF1 phase transition mediates stress adaptation and cell fate decisions. *Nat. Cell Biol.* **22**, 151–158 (2020).
 63. Persson, F., Lindén, M., Unoson, C. & Elf, J. Extracting intracellular diffusive states and transition rates from single-molecule tracking data. *Nat. Methods* **10**, 265–269 (2013).
 64. Hansen, A. S., Amitai, A., Cattoglio, C., Tjian, R. & Darzacq, X. Guided nuclear exploration increases CTCF target search efficiency. *Nat. Chem. Biol.* **16**, 257–266 (2020).
 65. Zentner, G. E. & Henikoff, S. High-resolution digital profiling of the epigenome. *Nat. Rev. Genet.* **15**, 814–827 (2014).
 66. Kasinathan, S., Orsi, G. A., Zentner, G. E., Ahmad, K. & Henikoff, S. High-resolution mapping of transcription factor binding sites on native chromatin. *Nat. Methods* **11**, 203–209 (2014).
 67. Tilly, B. C. *et al.* In vivo analysis reveals that ATP-hydrolysis couples remodeling to SWI/SNF release from chromatin. *Elife* **10**, (2021).
 68. Iurlaro, M. *et al.* Mammalian SWI/SNF continuously restores local accessibility to chromatin. *Nat. Genet.* **53**, 279–287 (2021).
 69. Schick, S. *et al.* Acute BAF perturbation causes immediate changes in chromatin accessibility. *Nat. Genet.* **53**, 269–278 (2021).

70. Kim, J. M. *et al.* Single-molecule imaging of chromatin remodelers reveals role of ATPase in promoting fast kinetics of target search and dissociation from chromatin. *Elife* **10**, (2021).
71. Jeronimo, C. *et al.* FACT is recruited to the +1 nucleosome of transcribed genes and spreads in a Chd1-dependent manner. *Mol. Cell* (2021) doi:10.1016/j.molcel.2021.07.010.
72. Nguyen, V. Q. *et al.* Spatiotemporal coordination of transcription preinitiation complex assembly in live cells. *Mol. Cell* (2021) doi:10.1016/j.molcel.2021.07.022.
73. Kwon, S. Y., Grisan, V., Jang, B., Herbert, J. & Badenhorst, P. Genome-Wide Mapping Targets of the Metazoan Chromatin Remodeling Factor NURF Reveals Nucleosome Remodeling at Enhancers, Core Promoters and Gene Insulators. *PLoS Genet.* **12**, e1005969 (2016).
74. Liu, Z. & Tjian, R. Visualizing transcription factor dynamics in living cells. *J. Cell Biol.* **217**, 1181–1191 (2018).
75. Wall, G., Varga-Weisz, P. D., Sandaltzopoulos, R. & Becker, P. B. Chromatin remodeling by GAGA factor and heat shock factor at the hypersensitive *Drosophila* hsp26 promoter in vitro. *EMBO J.* **14**, 1727–1736 (1995).
76. Chetverina, D., Erokhin, M. & Schedl, P. GAGA factor: a multifunctional pioneering chromatin protein. *Cell. Mol. Life Sci.* **78**, 4125–4141 (2021).
77. von Hippel, P. H. & Berg, O. G. Facilitated target location in biological systems. *J. Biol. Chem.* **264**, 675–678 (1989).
78. Schneider, I. Cell lines derived from late embryonic stages of *Drosophila melanogaster*. *J. Embryol. Exp. Morphol.* **27**, 353–365 (1972).
79. Cherbas, L. *et al.* The transcriptional diversity of 25 *Drosophila* cell lines. *Genome Res.* **21**,

- 301–314 (2011).
80. Tsai, S.-Y., Chang, Y.-L., Swamy, K. B. S., Chiang, R.-L. & Huang, D.-H. GAGA factor, a positive regulator of global gene expression, modulates transcriptional pausing and organization of upstream nucleosomes. *Epigenetics Chromatin* **9**, 32 (2016).
 81. Cattoglio, C. *et al.* Determining cellular CTCF and cohesin abundances to constrain 3D genome models. *eLife* vol. 8 (2019).
 82. Schwendemann, A. & Lehmann, M. Pipsqueak and GAGA factor act in concert as partners at homeotic and many other loci. *Proc. Natl. Acad. Sci. U. S. A.* **99**, 12883–12888 (2002).
 83. Gutierrez-Perez, I. *et al.* Ecdysone-Induced 3D Chromatin Reorganization Involves Active Enhancers Bound by Pipsqueak and Polycomb. *Cell Rep.* **28**, 2715–2727.e5 (2019).
 84. Duan, J. *et al.* CLAMP and Zelda function together to promote zygotic genome activation. *Elife* **10**, (2021).
 85. Kaye, E. G. *et al.* Differential Occupancy of Two GA-Binding Proteins Promotes Targeting of the Drosophila Dosage Compensation Complex to the Male X Chromosome. *Cell Rep.* **22**, 3227–3239 (2018).
 86. Sekiya, T., Muthurajan, U. M., Luger, K., Tulin, A. V. & Zaret, K. S. Nucleosome-binding affinity as a primary determinant of the nuclear mobility of the pioneer transcription factor FoxA. *Genes Dev.* **23**, 804–809 (2009).
 87. Brodsky, S. *et al.* Intrinsically Disordered Regions Direct Transcription Factor In Vivo Binding Specificity. *Mol. Cell* **79**, 459–471.e4 (2020).
 88. Chaharbakshi, E. & Jemc, J. C. Broad-complex, tramtrack, and bric-à-brac (BTB) proteins: Critical regulators of development. *Genesis* **54**, 505–518 (2016).

89. Mahmoudi, T., Katsani, K. R. & Verrijzer, C. P. GAGA can mediate enhancer function in trans by linking two separate DNA molecules. *EMBO J.* **21**, 1775–1781 (2002).
90. Paakinaho, V., Johnson, T. A., Presman, D. M. & Hager, G. L. Glucocorticoid receptor quaternary structure drives chromatin occupancy and transcriptional outcome. *Genome Res.* **29**, 1223–1234 (2019).
91. Biggin, M. D. Animal transcription networks as highly connected, quantitative continua. *Dev. Cell* **21**, 611–626 (2011).
92. Fisher, W. W. *et al.* DNA regions bound at low occupancy by transcription factors do not drive patterned reporter gene expression in *Drosophila*. *Proc. Natl. Acad. Sci. U. S. A.* **109**, 21330–21335 (2012).
93. Zaret, K. S. Pioneer Transcription Factors Initiating Gene Network Changes. *Annu. Rev. Genet.* **54**, 367–385 (2020).
94. Hansen, J. L. & Cohen, B. A. A Test of the Pioneer Factor Hypothesis. *bioRxiv* 2021.08.17.456650 (2021) doi:10.1101/2021.08.17.456650.
95. Johnson, T. A. *et al.* Conventional and pioneer modes of glucocorticoid receptor interaction with enhancer chromatin in vivo. *Nucleic Acids Res.* **46**, 203–214 (2018).
96. Heinz, S. *et al.* Simple combinations of lineage-determining transcription factors prime cis-regulatory elements required for macrophage and B cell identities. *Mol. Cell* **38**, 576–589 (2010).
97. Bier, E., Harrison, M. M., O'Connor-Giles, K. M. & Wildonger, J. Advances in Engineering the Fly Genome with the CRISPR-Cas System. *Genetics* **208**, 1–18 (2018).
98. Sharan, S. K., Thomason, L. C., Kuznetsov, S. G. & Court, D. L. Recombineering: a

- homologous recombination-based method of genetic engineering. *Nat. Protoc.* **4**, 206–223 (2009).
99. Zhang, Y., Schreiner, W. & Rong, Y. S. Genome manipulations with bacterial recombineering and site-specific integration in *Drosophila*. *Methods Mol. Biol.* **1114**, 11–24 (2014).
100. Groth, A. C., Fish, M., Nusse, R. & Calos, M. P. Construction of transgenic *Drosophila* by using the site-specific integrase from phage phiC31. *Genetics* **166**, 1775–1782 (2004).
101. Ranjan, A. *et al.* Live-cell single particle imaging reveals the role of RNA polymerase II in histone H2A.Z eviction. *Elife* **9**, (2020).
102. Schindelin, J. *et al.* Fiji: an open-source platform for biological-image analysis. *Nat. Methods* **9**, 676–682 (2012).
103. Vallotton, P. & Olivier, S. Tri-track: free software for large-scale particle tracking. *Microsc. Microanal.* **19**, 451–460 (2013).
104. Wieser, S. & Schütz, G. J. Tracking single molecules in the live cell plasma membrane-Do's and Don't's. *Methods* **46**, 131–140 (2008).
105. Loffreda, A. *et al.* Live-cell p53 single-molecule binding is modulated by C-terminal acetylation and correlates with transcriptional activity. *Nat. Commun.* **8**, 313 (2017).
106. Tatavosian, R. *et al.* Live-cell single-molecule dynamics of PcG proteins imposed by the DIPG H3.3K27M mutation. *Nat. Commun.* **9**, 2080 (2018).
107. Cattoglio, C., Darzacq, X., Tjian, R. & Hansen, A. S. Estimating Cellular Abundances of Halo-tagged Proteins in Live Mammalian Cells by Flow Cytometry. *Bio Protoc* **10**, e3527 (2020).
108. Omichinski, J. G., Pedone, P. V., Felsenfeld, G., Gronenborn, A. M. & Clore, G. M. The

solution structure of a specific GAGA factor-DNA complex reveals a modular binding mode.

Nat. Struct. Biol. **4**, 122–132 (1997).

109. Ramírez, F. *et al.* deepTools2: a next generation web server for deep-sequencing data analysis. *Nucleic Acids Res.* **44**, W160–5 (2016).

110. Wilkins, R. C. & Lis, J. T. GAGA factor binding to DNA via a single trinucleotide sequence element. *Nucleic Acids Res.* **26**, 2672–2678 (1998).

111. Zielke, N. *et al.* Fly-FUCCI: A versatile tool for studying cell proliferation in complex tissues. *Cell Rep.* **7**, 588–598 (2014).

112. Asha, H. *et al.* Analysis of Ras-induced overproliferation in *Drosophila* hemocytes. *Genetics* **163**, 203–215 (2003).